Zitierweise: *Angew. Chem. Int. Ed.* **2025**, *64*, e202503593
doi.org/10.1002/anie.202503593

Metal Halide Perovskites

Fluid Chemistry of Metal Halide Perovskites

Changshun Chen, Qing Yao, Jinpei Wang, Chenxin Ran, Lingfeng Chao, Yingdong Xia,* and Yonghua Chen**

Abstract: Solution-processed metal halide perovskites (MHPs) have been rapidly developed worldwide, with much attention to fluid dynamic, fluid crystallization, and fluid interfaces, all falling within the realm of fluid chemistry. It is widely recognized that the theory of fluid chemistry has been proven to provide an effective means for the improvement of perovskite crystallization and the enhancement of perovskite solar cells (PSCs) performance. In this review, the fluid behavior, microfluidic synthesis, and aging process of perovskite materials are first investigated, with emphasis on the related improvement methods and chemical mechanisms. Second, the internal crystallization chemistry, external interface chemistry, and the large-area PSCs based on the fluid chemistry are discussed. Finally, four specific directions for future studies of fluid chemistry of MHPs are proposed, aiming to harness the theoretical advantages of fluid chemistry and contribute to the industrialization of PSCs.

1. Introduction

Metal halide perovskite solar cells (PSCs) have achieved a power conversion efficiency (PCE) that is now competitive with that of silicon photovoltaic cells, owing to their versatility in molecular designs, lightweight nature, easy processability, and integration potential into diverse applications.[1–5] In comparison with traditional photoelectric devices, solution-processed devices benefit from the layer-by-layer solution process, which enables them to have high material utilization, low cost, and the potential for large-scale production.[6,7] Moreover, the crystallization activation energy barriers for perovskites are markedly lower.[8] Consequently, it is possible to fabricate highly crystalline perovskite thin films, which exhibit low densities of defects and reduce the production costs through various low-temperature solution-processed methods compared to silicon-based technologies.[9–12]

The performance of PSCs is heavily influenced by the intrinsic properties of the active materials, including the coverage, uniformity, and crystallinity of the deposited perovskite films, all of which are strongly affected by the deposition process of the active materials.[13,14] This process involves the fluid behavior of perovskite materials and the interaction between the chemical molecules, both of which determine the final properties of the deposited perovskite films.[15,16] However, most prior research has treated the macroscopic fluid motion and the intermolecular chemical reactions as separate phenomena, hindering a complete picture of perovskite phase transformation.

Fluid chemistry provides a comprehensive framework for investigating the phase transition process of perovskite materials, encompassing processes such as solvent evaporation, chemical coordination, surface flow, crystal growth, and interfacial reactions. This approach is beneficial for achieving the uniform large-area perovskite deposition and the continuity of crystallization chemistry.[17,18] Meanwhile, the study of fluid chemistry of perovskite materials offers an integrated understanding of fluid behavior and intermolecular interaction in chemical systems.[19] Through the investigation of these interactions, critical information on the crystallization kinetics, interfacial chemistry, and stability of perovskite materials during phase transition is revealed.[20–22] This contributes to our comprehension of the crystal transformation process of perovskite materials and the enhancement of perovskite device performance.[23–26]

In this review, fluid chemistry involving the quality of perovskite thin films and thus the performance of devices is summarized. We expand the understanding of perovskite crystallization beyond traditional static solution perspectives to the dynamic fluid considerations (Figure 1a).[27–30] We illustrate how various fluid strategies influence both internal crystallization and interfacial reactions in perovskite materials through their rheological behavior and layering properties (Figure 1b). We begin with the introduction of the fundamental characteristics of fluid behavior, which govern the surface morphology and internal defects of perovskite film. Subsequently, we explore fluid chemistry for internal crystallization represented by the solvent chemistry and additive engineering of perovskite solution, aiming to elucidate the evolution of perovskite crystal and chemical interaction within perovskite solution. We also investigate the fluid chemistry for interfacial reaction of perovskite materials during crystallization process,

[*] C. Chen, C. Ran
Frontiers Science Center for Flexible Electronics, Institute of Flexible Electronics (IFE), Northwestern Polytechnical University, 127 West Youyi Road, Xi'an 710072, China

C. Chen, Q. Yao, J. Wang, L. Chao, Y. Xia, Y. Chen
State Key Laboratory of Flexible Electronics (LoFE) & Institute of Advanced Materials (IAM), School of Flexible Electronics (Future Technologies), Nanjing Tech University (NanjingTech), 30 South Puzhu Road, Nanjing, Jiangsu 211816, China
E-mail: iamlfchao@njtech.edu.cn
iamydxia@njtech.edu.cn
iamyhchen@njtech.edu.cn

such as gas–liquid fluid interface, solid–liquid fluid interface, gas-intermediate phase interface, and liquid-intermediate phase interface. Finally, we discuss the preparation methods for large-area PSCs based on gas and liquid methods, which is crucial for understanding the perovskite phase transition, enhancing the performance of perovskite modules, and advancing industrial application.

2. Fluid Behavior and Stability

Fluid, a state of matter capable of freely changing shape and volume, is described by key parameters such as density, viscosity, surface tension, and thermal conductivity. Compared to solids, the intermolecular force between fluid molecules is weaker, allowing for fluid flow and deformation.[31–38]

Changshun Chen received his bachelor's degree in chemistry from Changchun University of Science and Technology in 2018. He is currently a PhD candidate in the Institute of Flexible Electronics, Northwestern Polytechnical University, Xi'an, China. His research areas focus on perovskite printing and large-area perovskite optoelectronic devices.

Qing Yao received her master's degree in materials engineering from Shandong University of Science and Technology in 2022. She is currently a PhD candidate in the Institute of Advanced Materials (IAM) & School of Flexible Electronics (Future Technologies), Nanjing Tech University. Her current research focuses on screen-printed high-efficiency perovskite solar cells.

Jinpei Wang received his master's degree in chemical engineering from Nanjing Tech University in 2020. He is currently a PhD candidate in the Institute of Advanced Materials (IAM) & School of Flexible Electronics (Future Technologies), Nanjing Tech University. His current research focuses on high-efficiency Sn–Pb perovskite solar cells and all-perovskite tandem solar cells.

Chenxin Ran received his PhD degree in electronic science and technology from Xi'an Jiaotong University in 2016 with Prof. Minqiang Wang. He worked as a visiting scholar from 2014 to 2015 with Prof. Liming Dai at Case Western Reserve University and as a lecturer at Xi'an Jiaotong University from 2016 to 2019. Now he is working as an associate professor at Northwestern Polytechnical University. His research interests include photophysics of Pb/Pb-free-based perovskite materials and their optoelectronic applications.

Lingfeng Chao received his BS degree in applied chemistry from Tangshan Normal University in 2016 and MS degree from the Institute of Advanced Materials (IAM), Nanjing Tech University in 2019. He received his PhD degree from the Institute of Flexible Electronics (IFE), Northwestern Polytechnical University. Now he works as a professor at Nanjing Tech University. His research interest is solvent engineering toward large-area production of perovskite solar cells.

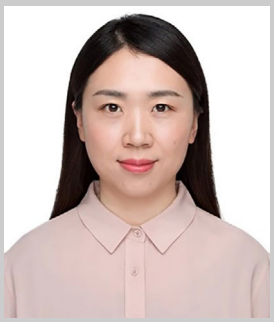

Yingdong Xia received her BE degree in macromolecular science and engineering from Hebei University in 2006 and the PhD degree in polymer chemistry and physics from Changchun Institute of Applied Chemistry, Chinese Academy of Sciences, in 2011. She then conducted her postdoctoral researche at Georgia Institute of Technology and Wake Forest University during 2011–2013. She is now a professor at Nanjing Tech University. Her current research interest is focused on organic light-emitting diodes, perovskite light-emitting diodes, and solar cells.

Yonghua Chen received his bachelor's degree in chemistry from Inner Mongolia University in 2006 and a PhD in polymer chemistry and physics from the Changchun Institute of Applied Chemistry, Chinese Academy of Sciences, in 2011. Afterward, he spent time at Wake Forest University and Case Western Reserve University as a postdoctoral researcher. He is currently a full-time professor at Nanjing Tech University. His research interests are organic and organic/inorganic hybrid optoelectronic materials and devices for flat panel displays and solid-state lighting, and for energy conversion.

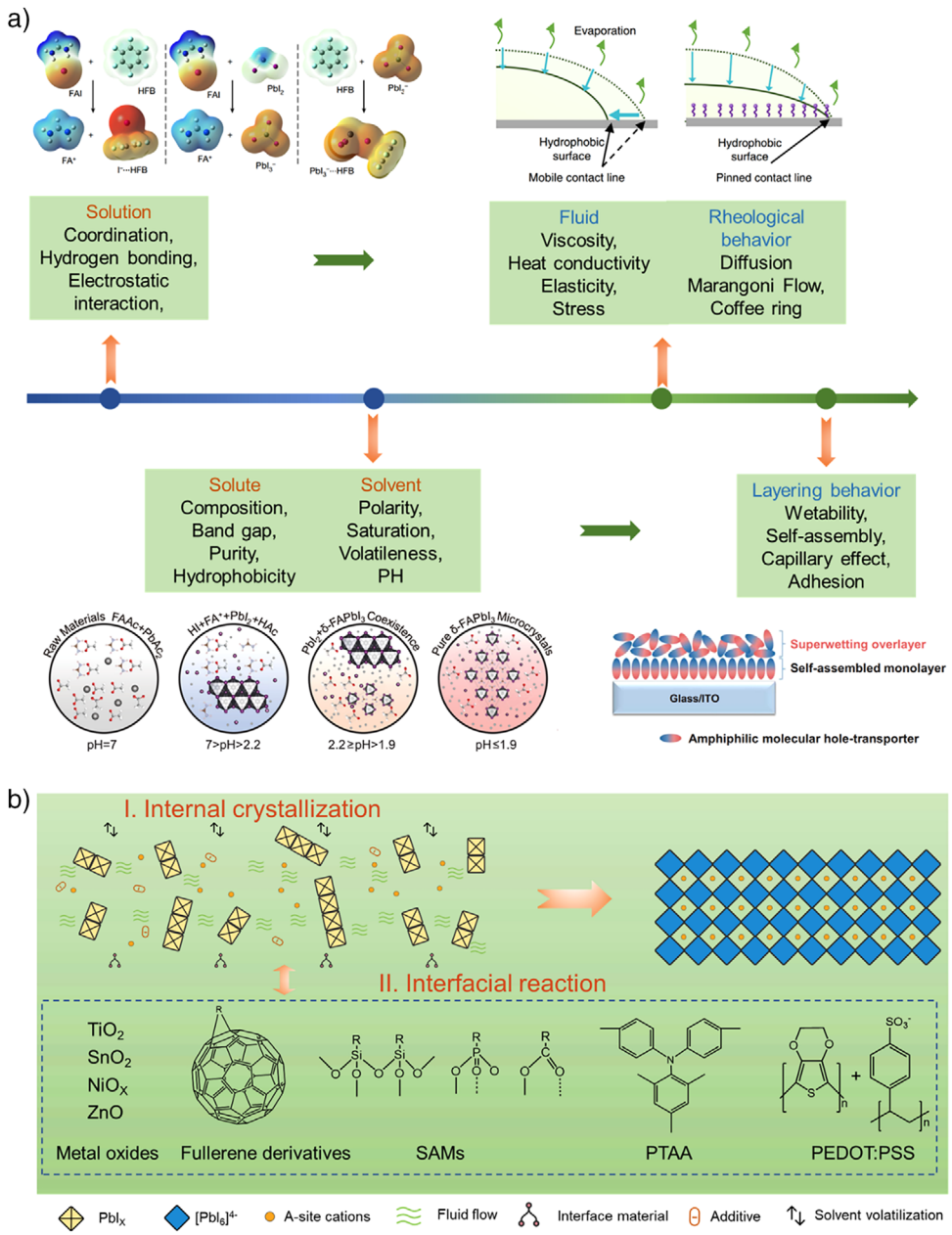

Figure 1. Perovskite solution and fluid. a) Factors affecting the perovskite crystallization process from solution view and fluid view, adapted from Refs. [27–30] with permission. b) Perovskite fluid chemistry based on internal crystallization and interfacial reaction.

Liquid fluid maintains a constant, incompressible volume and can develop free surfaces shaped by gravity or pressure. Inversely, gas fluid can be compressed or expanded, lacking a fixed volume and shape. The fluid behavior involves a range of phenomena, including spreading and shrinking, mass transport, heat transfer, and surface tension effects, under the influence of chemical materials. These factors collectively influence the initial flow behavior of perovskite materials on the substrate and the early perovskite phase transition process.[39–42]

2.1. Fluid Behavior of MHPs

In order to uncover the mechanisms governing the quality and performance of perovskite films, we first investigate the fluid behavior of MHPs.[43] Understanding these aspects is essential for optimizing crystallization processes and interfacial reactions, ultimately enhancing device efficiency and stability. As shown in Figure 2a,b, we broaden the study of perovskite crystallization from traditional static solutions to the dynamic fluid. The spreading of perovskite materials

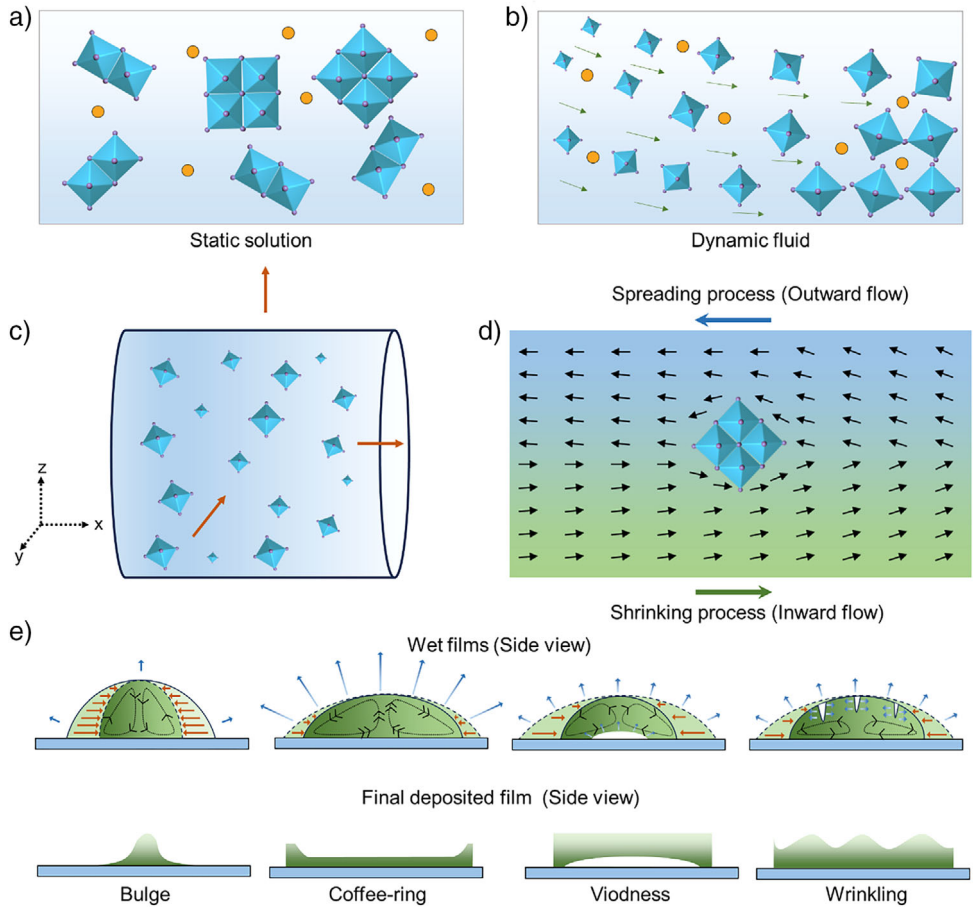

Figure 2. Perovskite fluid behavior. a) Static perovskite solution. b) Dynamic fluid flow of perovskite solid particles. c) 3D fluid flow channel during perovskite crystallization. d) Cross-section diagram of fluid motion channel. The overall motion can be decomposed into spreading process of outward flow and shrinking process of inward flow. e) Different morphologies of wet perovskite films and deposited perovskite films, including bulge, coffee-ring, voidness, and wrinkling.

involves the deformation and movement of the fluid under external forces.[44–49] In the early stage of perovskite solution contact with substrate, the fluid properties of the solvent, including surface tension and viscosity, determine the flow and distribution of the solute. Viscosity, as a less studied but extremely important physical parameter, was reported in our previous work and discussed in the next section of the article. The spreading of perovskite ink on solid surfaces is influenced by droplet diffusion dynamics.[50–55] Upon surface contact, spreading is driven by free energy, which is a function of surface tension and gravity. As the droplet reaches equilibrium on the contact line, satisfying the Young–Laplace equation:

$$\cos\ \theta_S = (\sigma_{SG} - \sigma_{SL})/\sigma_{LG}$$

where θ_S is the static advancing contact angle, and σ_{SG}, σ_{SL}, and σ_{LG} are the surface tension between solid and gas phase, the surface tension between solid and liquid, and the interfacial tension between liquid and gas, respectively.[56] Without substrate heating, the spreading process of perovskite ink is primarily influenced by the liquid–solid interface owing to the low gas volatilization rate. The charge transport layer beneath the perovskite film typically exhibits poor wetting properties with respect to the perovskite ink.[9,57] By integrating a small amount of surfactant additive into the perovskite ink, it becomes feasible to alter the ink flow dynamics and enhance the adhesion of the perovskite ink to the substrate materials.[58–60] L-α-phosphatidylcholine (LP) is studied for its impact on enhancing perovskite ink adhesion to hydrophobic substrate.[28] The addition of mere 20 ppm of LP can immobilize the intermediate-phase particles from moving toward perovskite islands, maintaining droplet coverage at nearly 100% during drying process. In addition, self-assembled monolayers (SAMs) have emerged as a pivotal strategy for regulating interfaces and enhancing the wettability of perovskite films, consequently leading to substantial improvements in the performance and stability of PSCs.[30,61–63] For instance, the amphiphilic molecular (2-(4-(bis(4-methoxyphenyl)amino)phenyl)-1-cyanovinyl)phosphonic acid (MPA-CPA) can reduce the buried interfacial defects and enhances perovskite crystallinity.[30] It forms a bilayer stack with a chemically anchored SAMs, promoting superwetting characteristics for the perovskite ink. The superwetting capability of MPA-CPA leads to a highly uniform perovskite film, contrasting with the challenges faced using polytriarylamine (PTAA) or nickel oxide (NiO_X).

As shown in Figure 2c, the motion of perovskite solid particles dispersed in the solvent during crystallization process can be simulated by fluid pipeline model. In the absence of external constraints, the movement of perovskite particles is often random along any direction. However, when the density, viscosity, volume, and other solution parameters are changed during solvent evaporation, the flow mode and order degree of perovskite particles in the pipeline will change accordingly. As shown in Figure 2d, Marangoni flow, a phenomenon characterized by fluid motion along the surface tension gradient of liquid, is observed when surface tension becomes unevenly distributed in perovskite wet film.[64–69] Besides, the solvent volatilization results in the outward spreading of the solute under the thermal field, both of which largely determine the uniformity of the deposited perovskite films. A mismatch between the solvent evaporation rate and Marangoni flow can result in morphological irregularities in the deposited perovskite film, such as middle bulging (inward strong Marangoni flow), coffee ring (too fast solvent evaporation rate), bottom voidness (surface-interface energy difference), and surface wrinkling (stress relaxation) (Figure 2e). For example, by employing a binary solvent strategy with solvents such as *n*-octane and *n*-hexane for perovskite inks, solvent flow can be finely adjusted by manipulating the mixing ratio, thus alleviating issues like inward Marangoni flow induced by temperature gradient and promoting outward Marangoni flow for uniform solute redistribution. Furthermore, the triple co-solvent system consisting of DMF, DMSO, and NMP can improve the wettability of the perovskite ink at Me-4PACz due to the enhanced solid–liquid binding energy, which contributes to the uniform layer and high-performance perovskite device.[70] The surface tension, viscosity, and inertia properties of inks significantly influence the rheological behavior of stable microscale liquid jets and droplets. These properties can be evaluated using the Z value of the solvents,[71] a dimensionless number that reflects fluid printability and guides the optimization of perovskite printing process.

The coffee-ring effect (CRE) describes the accumulation of solute at the edge of a perovskite film during deposition, driven by the higher evaporation rate of solvent at the edge of perovskite film.[72,73] This effect can significantly alter the uniformity and optoelectronic properties of the perovskite film. Various approaches can be employed to reduce the CRE of perovskite film, including solvent regulation, surface treatment, and the introduction of additives.[28,74,75] For example, the poly(ethylene glycol) diacrylamide (PEG-DAM) framework can regulate the intensity of Marangoni flow and lateral thermal capillary flow during droplet evaporation, effectively alleviating CRE. Besides, the increased viscosity suggests partial cross-linking of polymer monomers for enhanced structural properties. The formation of perovskite film is profoundly influenced by stress, which leads to common morphological changes such as buckling and wrinkling, potentially resulting in mechanical failure under compressive stress.[76–80] These manifestations encompass blistering or a wormlike appearance resulting from isotropic compressive stress.[81] The formation mechanism of wrinkling has a typical two-layer model, specifically, under the action of antisolvents, perovskite films will form a viscous layer and a solid layer. Different antisolvents will lead to changes in the stress and crystallization behavior of perovskite, which will cause different wrinkles. However, careful manipulation of these microscopic deformations in perovskite film can actually improve the performance of PSCs.[82,83] For instance, micro-wrinkling in perovskite layer has been utilized to enhance charge carrier transport efficiency.[78,84,85] By manipulating the temperature-dependent miscibility between DMSO and diethyl ether (DE), precise control over the microstructure of perovskite films is achieved.

2.2. Microfluidic Synthesis of MHPs

The theory of fluid chemistry, which focuses on the regulation of fluid motion and mass transfer in chemical reactions, has demonstrated considerable potential in the synthesis of advanced materials for photovoltaic and optoelectronic applications. Perovskite quantum dots (PQDs), known for their outstanding optoelectronic properties, have emerged as promising candidates for light-emitting diodes (LEDs).[86] However, traditional batch synthesis methods, such as hot injection, are often limited by inefficient mass transfer and poor control over reaction conditions, often resulting in broad particle size distributions and poor reproducibility, which hinder large-scale production. To address these challenges, microfluidic reaction systems guided by fluid chemistry principles have been developed to enable precise manipulation of fluid dynamics and reaction parameters within microscale channels.[87] By enhancing mixing efficiency, mass and heat transfer rates, and reaction kinetics, microfluidic approaches facilitate rapid nucleation and uniform growth of PQDs, effectively suppressing aggregation and size nonuniformity.

A modular microfluidic platform has been constructed to achieve precise control over the synthesis of PQDs.[88] As shown in Figure 3a,b, this system integrates a translational three-port flow cell with modular reactor extensions, allowing flexible operation in both single-phase and multiphase flow modes. In the multiphase configuration, segmented droplets are generated, which enhance mixing efficiency and minimize axial dispersion. By adjusting the flow rate and residence time, the nucleation and growth of $CsPbBr_3$ nanocrystals can be precisely regulated. As shown in Figure 3c, higher flow velocities are associated with reduced residence times, resulting in the formation of smaller nanocrystals with a blue-shifted photoluminescence emission. Compared to single-phase flow, the two-phase system exhibited improved uniformity in particle size and optical properties, offering great potential for scalable and reproducible synthesis of PQDs with tunable optoelectronic properties (Figure 3d).

In addition, a microfluidic blow spinning strategy has been developed to fabricate fibrous nanoreactors, enabling the continuous and large-scale production of ligand-free and highly stable PQDs with enhanced PL stability and emission tunability.[87] In a recent work, microfluidic photo-flow reactors have been employed to investigate the mechanisms of photo-induced anion exchange reactions (PIAER) in PQDs, allowing for precise bandgap engineering.[89] This microfluidic

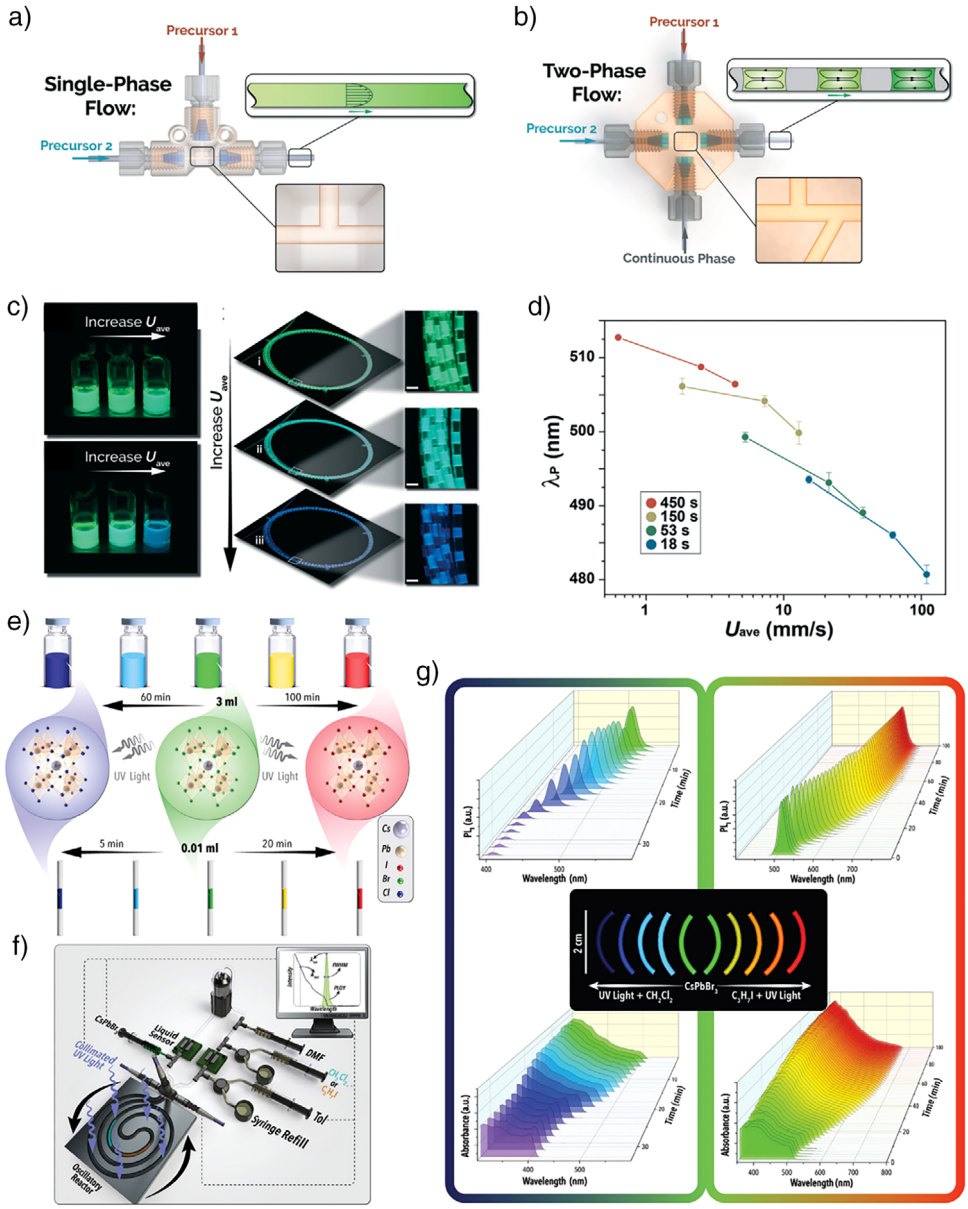

Figure 3. Microfluidic strategies for the controlled synthesis of PQDs. a) Schematic of a T-junction for single-phase flow. b) Multiphase flow format implementing Y-junction plug formation. c) Effect of single and multiphase microfluidic flow on PQDs synthesis. d) Influence of flow velocity and residence time on the PL peak wavelength of $CsPbBr_3$ QDs, a–d) adapted from Ref. [88] with permission. e) Comparison between batch and microfluidic systems for PIAER. f) Microfluidic platform for high-throughput in situ investigation of PIAER in PQD synthesis. g) Real-time optical analysis of PIAER during microfluidic synthesis of PQDs, e–g) adapted from Ref. [89] with permission.

approach significantly accelerates the anion exchange process and reduces material consumption compared to conventional batch methods, offering a scalable and material-efficient route for producing compositionally tunable PQDs. As shown in Figure 3e, microscale flow reactors allow for more efficient PIAER by reducing reaction time and volume while ensuring uniform photon exposure. Additionally, an automated single-droplet photo-flow microfluidic platform has been established to intensify the reaction process, minimize reagent consumption, and enable real-time in situ monitoring of PIAER (Figure 3f). This system ensures homogeneous light distribution and continuous mixing within reactive droplets, which is essential for maintaining reaction uniformity. In situ UV–vis absorption and photoluminescence spectral monitoring reveal the dynamic evolution of PIAER between $CsPbBr_3$ nanocrystals and generated halide anions (Figure 3g), providing precise control over chemical composition and bandgap tuning throughout the reaction. In another research work, core-shell nanofiber structures prepared by microfluidic electrospinning have facilitated the in situ formation of stable PQDs with improved PL quantum yields and environmental durability.[90] Additionally, microfluidic technologies have been employed to uncover the mechanisms of nanocrystal nucleation and growth, enabling real-time monitoring

and precise control of reaction parameters for high-quality PQD synthesis.[91] Furthermore, robust polyvinylpyrrolidone (PVP)-encapsulated $CsPbBr_3$ PQD powders have been synthesized by microfluidic electrospinning, demonstrating high stability and potential applications in 3D printing.[92] The microfluidic technology has been widely applied in the synthesis and process optimization of PQDs, offering precise control over reaction kinetics, scalability, and material quality.[93] Based on the aforementioned studies, it can be concluded that although microfluidic reaction systems guided by fluid chemistry principles have been predominantly applied to the synthesis of PQDs, their precise regulation of mass transfer, heat transfer, and reaction kinetics provides valuable insights for investigating phase transitions and crystallization mechanisms in perovskite thin films.[94]

2.3. Fluid Stability of Perovskite Materials

In order to provide a comprehensive overview of the stability of the perovskite materials, this section analyzes the effects of the solute purity, the solubility of the solute, the interplay between solute and solvent, and the chemical reactions among different solutes.[95–97] These elements collectively shape the state of the precursor ink, thereby exerting a profound impact on the final perovskite film. As shown in Figure 4a, the reversible acid–base decomposition process results in the deprotonation of organic ammonium R^+ and the formation of volatile ammonium R, ultimately altering the stoichiometric ratio of R/PbI_2 in the precursor ink and damaging the stability of PSCs.[98–100] In the perovskite ink with MAI and FAI, FAI continuously consumes MA, leading to the formation of condensation products. The nucleophilicity of the lone-pair electrons on the N atom in MA and the electrophilic nature of the imine bond in FAI drive an addition–elimination reaction, resulting in the formation of *N*-methyl FA (MFA) and *N*,*N*-dimethyl FA (DMFA). Regarding solvents, the DMF/DMSO system remains the classical solvent choice that is extensively employed in the fabrication of high-efficiency devices.[101] However, there are still several challenges. Firstly, as shown in Figure 4b, DMF readily undergoes hydrolysis, leading to adverse effects on the pH of precursor ink.[102] Secondly, despite the widespread use of FA^+ in high PCE and stable PSCs, the degradation is susceptible due to proton transfer with DMF and DMSO.[103] In the aprotic solvent GBL/DMSO system, solvent stability can be improved due to the fewer negative side reactions.[104] Besides, the coordination between solvent/additive and perovskite raw material can potentially extend the service life of perovskite ink.[105–108] As shown in Figure 4c, a biomass-derived solvent mixture composed of gamma-valerolactone (GVL, donor number (D_N): 18.1, boiling point (BP): 207 °C, saturated vapor pressure (SVP) 0.235 mmHg) and *n*-butyl acetate (BAc, D_N: low, BP: 126 °C, 11.5 mmHg) has been demonstrated to facilitate the solution-based fabrication of high-quality formamidinium lead iodide ($FAPbI_3$) perovskite. The stability of the perovskite ink is enhanced for up to a year by the formation of high-valence $[PbI_x]^{2-X}$ complexes and the strong interaction between GVL and FA^+ cations. Compared with DMF (D_N: 26.6, BP: 153 °C, 2.7 mmHg): DMSO (D_N: 29.8, BP: 189 °C, 0.6 mmHg), the GVL has a lower donor number, can form a higher high-valence $[PbI_x]^{2-X}$ with PbI_2 and a stronger interaction with FA^+ according to the hard–soft acids–bases theory. The facile formation of α-$FAPbI_3$ films from GVL based precursor solutions suggests that this solvent effectively reduces the energy barrier for the transformation of $[PbI_x]^{2-X}$ + FAI to the black-phase perovskite.[105] This solvent promotes easier formation of 3D corner-sharing octahedral frameworks, enabling the attainment of α-$FAPbI_3$ even at room temperature.

Impurity in perovskite raw materials may introduce additional defects into perovskite films, thereby leading to accelerated degradation of the perovskite solution and the formation of harmful by-products.[109] The reduction in calcium ions, which are the primary impurity in the solution, has been shown to significantly decrease carrier trap states.[29] As shown in Figure 4d, H_2O has a high median lethal dose (LD_{50}) value and can dissolve PbI_2 in the presence of I^- ions. As shown in Figure 4e,f, by adding an appropriate amount of HI (PH < 1.9), the octahedral framework of $FAPbI_3$ can be stabilized and the solubility of $FAPbI_3$ can be reduced, and the large-scale aqueous phase synthesis of $FAPbI_3$ perovskite microcrystals can be successfully achieved. For another example, excessive amount of PbI_2 can impair the efficiency and stability of perovskite devices. However, research has demonstrated that a minor concentration of PbI_2 can effectively passivate defects within perovskite films and enhance carrier transport, attributed to the P-type semiconductor properties of PbI_2.[110,111]

Perovskite solutions prepared using ionic liquid solvents usually exhibit outstanding moisture stability, which is derived from the high viscosity of ionic liquid preventing the invasion of water molecules and inhibiting the deprotonation process of perovskite (Figure 4g). In addition, the ionic liquid has a rich hydrogen bond network structure that stabilizes the Pb–I octahedron through C═O─Pb chelation, and effectively prevent the aggregation and precipitation of PbI_2.[100,112,113] As shown in Figure 4h, ionic liquids are products of the reaction between Brønsted acids and Brønsted bases. As a common Brønsted base, MA participates in perovskite phase formation and limits device performance improvements. Therefore, it is necessary to develop new FA-based ionic liquids to further extend the applicability of these solvents in high-performance perovskite devices.

3. Fluid Chemistry for Internal Crystallization of MHPs

The intricate chemical dynamics occurring within perovskite ink involve a series of complex and continuous fluid reactions, including dissolution, coordination, complexation, nucleation, and growth.[114,115] In shaping the crystal quality of perovskite, solvent chemistry and additive engineering play crucial roles. These factors regulate nucleation and growth dynamics by forming chemical and hydrogen bonds, thereby influencing the film morphology and structural properties of the perovskite material. This precise manipulation

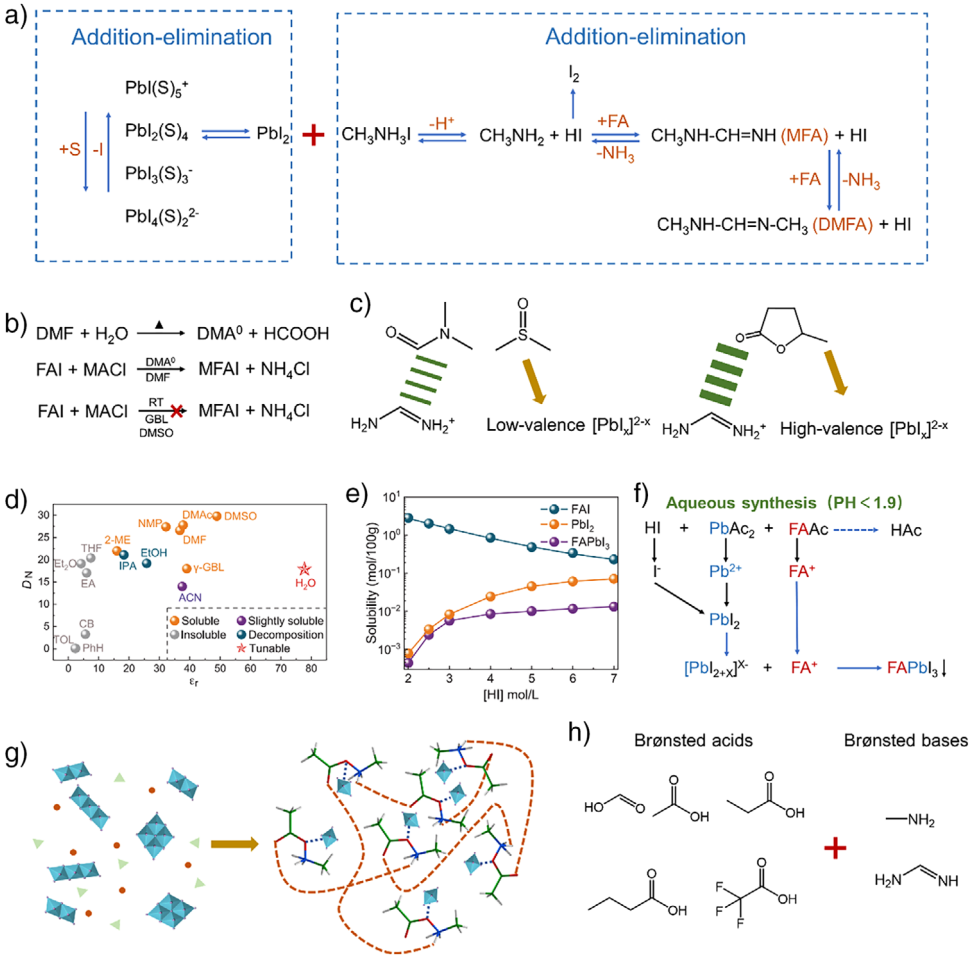

Figure 4. Fluid stability of perovskite ink. a) The equilibria established in solution around PbI_2, MAI, and FAI species, adapted from Ref. [95] with permission. b) The degradation of DMF into dimethylamine and formic acid in the presence of H_2O. c) Comparison of the DMF: DMSO-based and GVL-based perovskite inks, adapted from Ref. [105] with permission. d) The relations between Gutmann donor number (D_N), dielectric constant (ε_r), and median lethal dose (LD_{50}) for the solvents. e) HI concentration-dependent solubility of FAI, PbI_2, and $FAPbI_3$. f) Chemical reaction route for the synthesis of $FAPbI_3$ by the aqueous phase method, d–f) adapted from Ref. [29] with permission. g) Mechanism of excellent environmental stability of ionic liquid perovskite ink. h) Synthesis of protic ionic liquid based on methylamine and formamidine groups.

at the molecular level holds considerable potential for enhancing the performance and stability of perovskite-based devices.[116,117]

3.1. Perovskite Solvent Chemistry Based on Fluid Reaction

The selection of solvent significantly impacts various fluid properties of perovskite ink, including solubility, boiling point, freezing point, density, acidity, viscosity, surface tension, and polarity.[118,119] Solvents play essential roles in dispersion and bonding within perovskite ink, where the interaction strength between the solvent and solute predominantly shapes crystal structure characteristics and molecular dynamics.[120,121] An alternative approach is utilized to modulate reaction kinetics through the anion–π interaction between AX and hexafluorobenzene (HFB). The interaction collaborates to establish "dual-site regulation," delicately controlling the AX and BX_2 reaction without generating perovskite intermediates (Figure 5a).[27] The resultant $FAPbI_3$ film exhibits reduced defects, long wavelength absorption moving and high phase purity. The DFT calculations reveal favorable iodine anion interaction with HFB due to overlapping electron clouds and iodine–carbon distance shorter than their van der Waals radii sum. As shown in Figure 5b, the PbI_2 in dimethylformamide (DMF) displays an absorption peak at 285 nm related to PbI^+(DMF). Addition of HFB eliminates the PbI_3^-(DMF) peak and significantly reduces the PbI_2(DMF) peak, suggesting substantial inhibition of iodine–lead interaction by HFB. In the FAI…HFB…PbI_2 three-component system, the theoretical chemical equation is shown in the inset diagram. Employing this strategy, the high PCE of 26.07% is achieved. The 1,2-dimethoxyethane (DME) or isopropyl acetate (IA) is used to balance between solvation (i.e., the achievement of sufficient solubility of precursors) and desolvation (i.e., the promotion of rapid crystallization of films) processes during perovskite synthesis.[122,123] The polarity and hydrogen-bonding capacity of these cosolvents synergistically enhance their solvation power, thus facilitating

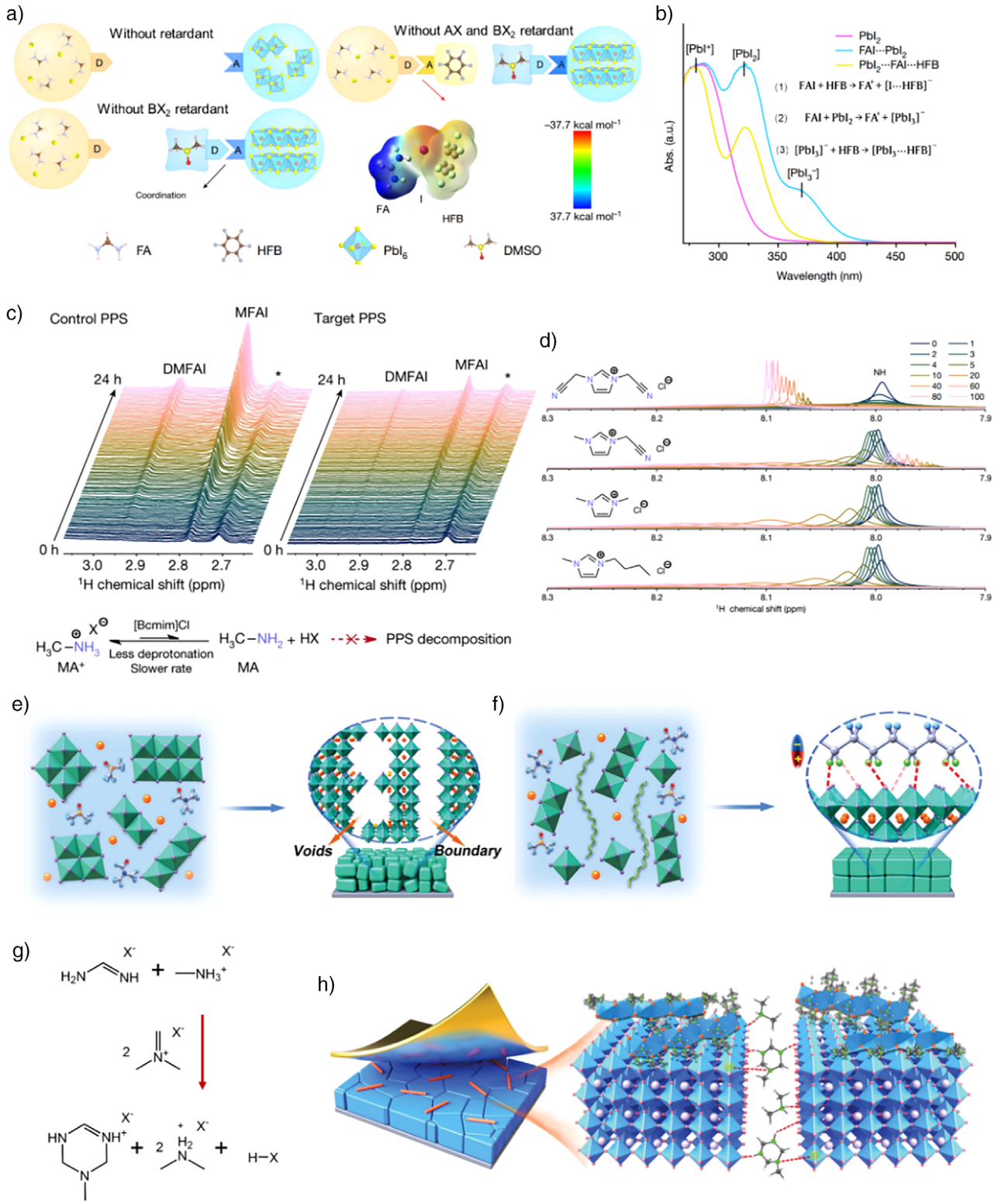

Figure 5. The solvent chemistry and additive engineering of internal crystallization of perovskite materials. a) Schematic illustration of using extra anion–π interactions as the HFB retardant in perovskite ink. b) The UV–vis absorption spectra of PbI_2, FAI···PbI_2, and FAI···PbI_2···HFB, a) and b) adapted from Ref. [27] with permission. c) ^{1}H NMR spectra of the perovskite precursor solution degradation at 60 °C for 24 h and the mechanism of the [Bcmim]Cl$^-$-mediated stabilization. d) ^{1}H NMR spectra of the interaction between MACl and four ionic liquids, c) and d) adapted from Ref. [135] with permission. e) The crystallization for control film without β-pV2F. f) The mechanism of β-pV2F for reducing perovskite formation energy and improving film quality, e) and f) adapted from Ref. [81] with permission. g) The chemical reaction for the formation of the dimethylmethyleneiminium ([MTTZ]$^+$) and dimethylammonium ([DMA]$^+$) cations. h) The functions of [MTTZ]$^+$ and [DMA]$^+$ within the 3D perovskite matrix, g) and h) adapted from Ref. [136] with permission.

perovskite ink dissolution. Furthermore, the crystallization of well-defined intermediate film is accelerated by the low-solvation cosolvents, resulting in the production of higher-quality perovskite films compared to those synthesized with DMF.

3.2. Perovskite Additive Engineering Based on Fluid Reaction

To systematically summarize the role of additives in modulating the crystallization and growth processes of perovskite materials, this section evaluates how specific additives enhance crystal quality, mitigate defects, optimize interface structures, and adjust band structures. These modifications improve the overall performance and stability of perovskite devices.[124–127]

Some specialized passivators and additive materials are systematically summarized, highlighting specific molecular designs and possible passivating mechanisms.[128] For example, ionic liquids serve multifaceted purpose, acting as a solvent, additive, and passivator simultaneously.[128–130] Their multifunctional properties have been extensively explored in stabilizing precursor inks and modulating the crystallization kinetics.[131,132] The optimization of perovskite fabrication through the inclusion of additives like ionic liquids results in the creation of perovskite materials exhibiting improved device efficiency and stability.[131–133] This improvement is attained through defect passivation, enhanced crystallinity and phase purity, along with the suppression of film decomposition.[134] A synergistic strategy, employing methylammonium chloride (MACl) as the dopant, along with the addition of a Lewis basic ionic liquid 1,3-bis(cyanomethyl)imidazolium chloride ([Bcmim]Cl), effectively hinders the degradation of perovskite ink and the aggregation of MACl.[135] Figure 5c illustrates the decomposition of mixed FA^+/MA^+ PPSs via a condensation reaction, yielding MFAI and DMFAI as principal products. However, proton exchange and relaxation reduction indicate inhibited MA^+ deprotonation to MA upon the introduction of 0.6 mol% [Bcmim]Cl, thus impeding the condensation reaction between MA^+ and FA^+. Figure 5d presents several model NMR spectroscopic experiments suggesting a notable broadening of the MA^+ cation NH peak in ^{1}H NMR spectra upon adding [Bcmim]Cl to a MACl solution. The certified PCE of the target perovskite modules reached 23.30% based on the interaction between [Bcmim]Cl and MACl.

In the pursuit of enhancing the performance of perovskite solar cells, significant improvements in the morphological characteristics of perovskite films were achieved through the incorporation of β-poly(1,1-difluoroethylene) (β-pV2F).[81] As shown in Figure 5e,f, the ordered dipolar structure of β-pV2F interacts with perovskite precursors, reducing the formation energy of the black photoactive phase. This interaction promotes the growth of a low-defect crystalline film with larger grain sizes (480 nm vs. 400 nm), fewer voids, and enhanced crystallinity. The surface roughness of perovskite film decreases from 54.4 to 41.1 nm, improving charge transport layer coverage. The consistent film thickness ensures optimal light absorption while maintaining high packing density. Additionally, β-pV2F suppresses ion migration and enhances hydrophobicity, leading to better interfacial charge extraction and stability. These improvements highlight β-pV2F-role in achieving superior morphological control and enhanced performance under varying thermal conditions. In situ cation formation presents a promising approach to enhance the stability of perovskite solutions and modules.[136] As shown in Figure 5g, the dimethylmethyleneiminium ($[Dmei]^+$) can react with MA^+ and FA^+ cations in perovskite solutions to form dimethylammonium ($[DMA]^+$) and 2,3,4,5-tetrahydro-1,3,5-triazin-1-ium ($[MTTZ]^+$) cations. As presented in Figure 5h, the $[MTTZ]^+$ cation stabilizes the resulting perovskite structure, raises the iodine vacancy formation energy, and improves film crystallinity, leading to a certified module PCE of 23.2%.

4. Fluid Chemistry for Interfacial Reaction of MHPs

The inherent flow and exchange properties of fluid endow them with the capability to facilitate rapid chemical reactions. The typical interfacial chemistry of perovskite encompasses reactive adsorption, surface modification, vapor deposition, heterostructure reconstruction, and other processes. Given the intense chemical reaction chemical at fluid interfaces, it is essential to analyze perovskite interface reactions from the perspective of fluid chemistry.

As shown in Figure 6, typical phase state of perovskite is categorized into perovskite gas-fluid, perovskite liquid-fluid, intermediate phase and solid, in which perovskite intermediate phase can be further divided into strong molecular diffusion intermediate phase and weak molecular diffusion intermediate phase according to the molecular diffusion capacity. Perovskite intermediate phase with strong diffusion is in the early stage of crystallization because it contains more solvents, perovskite materials will rearrange on the substrate with the evaporation of solvents and show strong remodeling. The perovskite intermediate phase with weak diffusion contains small amounts of solvent or solvent-free (such as mesophase for thermal evaporation), but still have great potential for movement and diffusion at the molecular level. The perovskite phase transition from liquid fluid or gas fluid to intermediate phase is a sensitive and rapid process, which can be induced by external gases, external liquids and solid molecules. These means can yield a range of beneficial effects, including enhancing the crystallization process of perovskite, passivating defects, inhibiting ion migration, constructing internal electric field, modifying energy level, improving the performance and stability of perovskite devices.

4.1. Interfacial Chemistry of Liquid Fluid

4.1.1. Gas–Liquid Fluid Interface

To systematically analyze the chemical reactions occurring at the gas–liquid fluid interface, this section examines how external gases interact with perovskite liquid films. The effects of gas extraction and pressing on solvent evaporation and

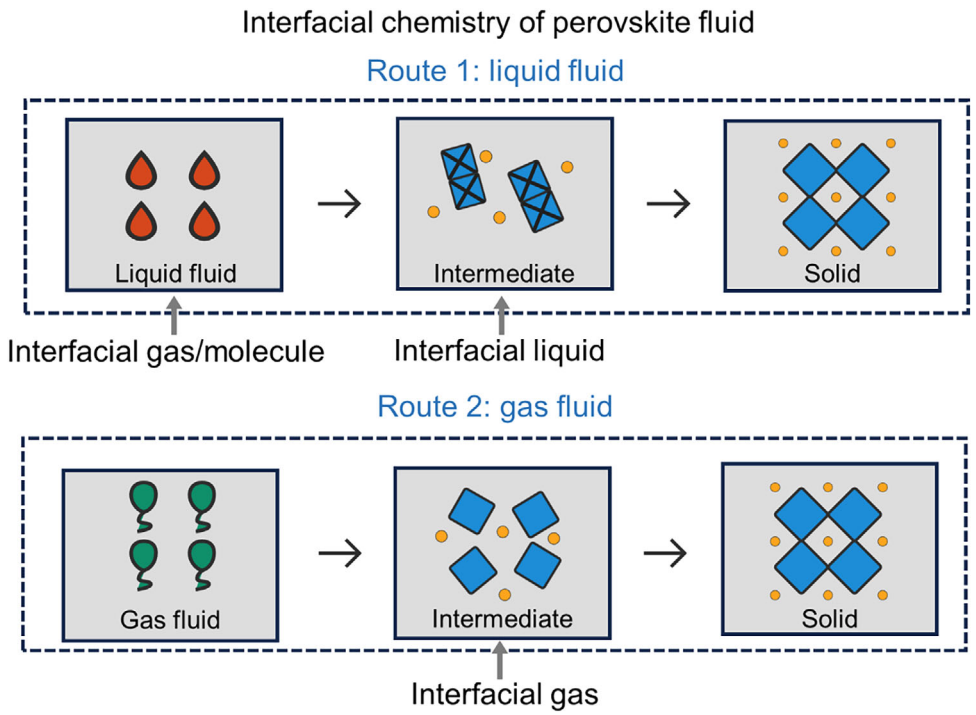

Figure 6. The interfacial chemistry of perovskite materials based on liquid fluid and gas fluid. Schematic diagram of liquid fluid, gas fluid, strong molecular diffusion intermediate phase and weak molecular diffusion intermediate phase, and solid perovskite depending on the ability of molecular diffusion. Perovskite interfaces can be classified into the following four categories according to different perovskite phase transition mechanisms and induction methods, including the gas–liquid fluid interface, the solid–liquid fluid interface, the liquid-intermediate phase interface, and the gas-intermediate phase interface.

crystallization are detailed, highlighting the importance of these interactions in enhancing film quality and device performance. As shown in Figure 7a, external gas interactions with perovskite liquid fluid films in two primary modes: extraction and pressing. Among these, vacuum-flash processing (VSP) stands out as a prevalent gas-fluid extraction technique, commonly applied to initial perovskite films.[137,138] The mechanical schematic of the two gas–liquid fluid interfacial reaction is shown in Figure 7b, the VSP facilitates solvent evaporation and expedites the crystallization of perovskite intermediate phases, leading to the smooth and high-crystallinity perovskite films. As shown in Figure 7c, the external gas press on the solid perovskite films serves dual purposes. First, the utilization of gas streams, including N_2, Ar_2, and air, facilitates a rapid transition to perovskite intermediates, thereby significantly accelerating perovskite crystallization.[139–141] Second, employing reactive gases like NH_3, CH_3NH_2, Cl_2–CF, Br_2, NH_4F, H_2O (fewer), CS_2, CO_2, O_3 enables participation in chemical displacement reactions within the perovskite liquid fluid, effectively addressing perovskite defects, eliminating grain boundaries, rearranging energy level, and secondary growth.[123,142–155] Additionally, certain perovskite raw materials release gas upon evaporation onto the surface of 3D perovskite films, thereby reducing interface recombination.[156,157] On the contrary, the O_2 and I_2 can lead to destructive decomposition of perovskite films, thereby affecting the performance of perovskite devices.[158,159]

Due to differences in chemical properties, FA and MA perovskites exhibit distinct gas induction strategies. As shown in Figure 7d, the volatile aliphatic methylamine (MA^0) significantly enhances the quality of MA-based films as coordinating ligand solvent or post-healing gas.[145,160] However, due to the degradation of the FA-perovskite using the MA^0 gas-related methods, the underlying chemical reactions between aliphatic amines/formamidine (FA^0) gases and FAI salt are studied.[143] The breakdown of FA-containing perovskites in aliphatic amine environments is due to a transimination reaction between FA^+ and aliphatic amines, leading to the generation of NH_3. The imine bond in the formed MFAI can carry out the second transimination reaction with MA^0 to form DMFAI. Similarly, when FAI powders are treated with EA^0, PA^0, and BA^0 gases, the transimination reaction occur with the formation of DEFAI, DPFAI, and DBFAI, respectively. The addition–elimination reaction between FA^0/RA^0 gases and FAI inspired the development of an NH_3 gas post-treatment strategy. This approach is based on the reversible adsorption–desorption reaction between NH_3 and FAI, by which defects in the perovskite films can be effectively repaired. Specifically, the NH_3 adsorbed $FAPbI_3$ will first become liquid, and then gradually change to a transparent crystal shape during the desorption process, and finally the completely desorbed perovskite material return to its initial mass. In the reversible absorption–desorption process, the crystallinity of the perovskite films is improved, and the formation of the undesired δ-phase is effectively suppressed. In contrast, MA^0 tends to undergo harmful chemical reactions with FAI, leading to irreversible processes that fail to provide effective defect healing for the perovskite films. Based on

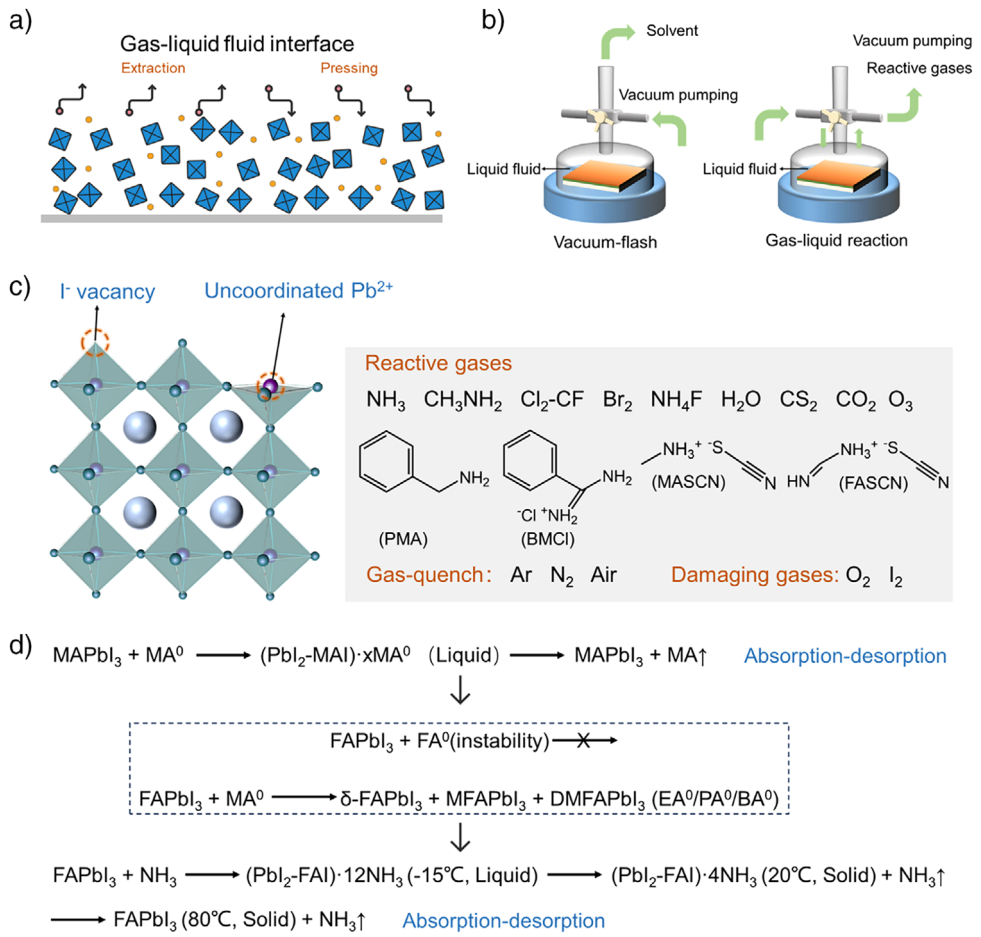

Figure 7. The chemistry reaction of the gas–liquid fluid interface. a) The schematic diagram of the gas–liquid fluid interface by gas extracting and pressing. b) Schematic diagram of the operation of vacuum-flash and gas–liquid fluid reaction. c) The defect types of perovskite materials and the gases with different effects on perovskite crystallization process, including reactive gases, gas-quench gases, and damaging gases. d) The chemical reactions and the ion exchange reactions between $MAPbI_3$ and RA^0 molecules. The chemical reactions and the ion exchange reactions between $FAPbI_3$ and RA^0 molecules (R refers to H, Me, Et, *n*-Pr, or *n*-Bu, etc.), and the interaction of NH_3 with FA-based perovskite ink, which is measured by the absorption and desorption behavior of MAI-MA^0, FAI-MA^0, and FAI-NH_3.

this NH_3/$FAPbI_3$ repairing strategy, the champion devices achieve remarkable PCE of 20.61% for large-area PSCs. Besides, the chemical reaction at the gas–liquid fluid interface can mitigate the limitations of the traditional liquid method, thus facilitating perovskite material growth along a particular plane.[161–166]

4.1.2. Solid–Liquid Fluid Interface

The solid–liquid fluid interface is comprehensively investigated, with an emphasis on how bottom solid materials, such as SAMs and surfactants, influence the motion behavior of perovskite materials and the carrier transport characteristics of the film (Figure 8a). The aggregation, dispersion, and stability of these materials are examined to understand their impact on device performance.

As shown in Figure 8b, the optimization of SAMs materials mainly focuses on the spacer, functional head group, anchoring group, and additives. These strategies significantly affect the aggregation, dispersion, carrier transport, and stability of SAMs materials.[167] For example, PTAA with a SAM suppresses the interfacial nonradiative recombination and improvement of perovskite spreading and crystallization, enabling improved performance in the record-efficiency all-perovskite tandem solar cells (TSCs). Since then, SAMs such as Me-4PACz, 2PACz, and MeO-2PACz have been widely adopted in efficient PVSK-TSCs.[8,168] These results indicate that crystallization regulation at the time solid–liquid fluid interface and carrier management enable the improved device performance and commercialization potential.

The aggregation effect of SAMs materials will lead to poor wettability and flow characteristics of perovskite solutions, Me-4PACz and multiple aromatic carboxylic acid 4,4′,4″-nitrilotribenzoic acid (NA) can enhance the heterojunction interface.[169] As shown in Figure 8c, NA-Me shows better distribution than Me-4PACz. Since Me-4PACz is able to interact with triphenylamine of NA molecules, it is beneficial to reduce nonradiative recombination at the NiO/perovskite interface. As shown in Figure 8d, At the same time, compared with benzoic acid (BA) and trimesic acid (TA), the carboxylic acid adsorption ratio of NA-Me and the surface coverage of

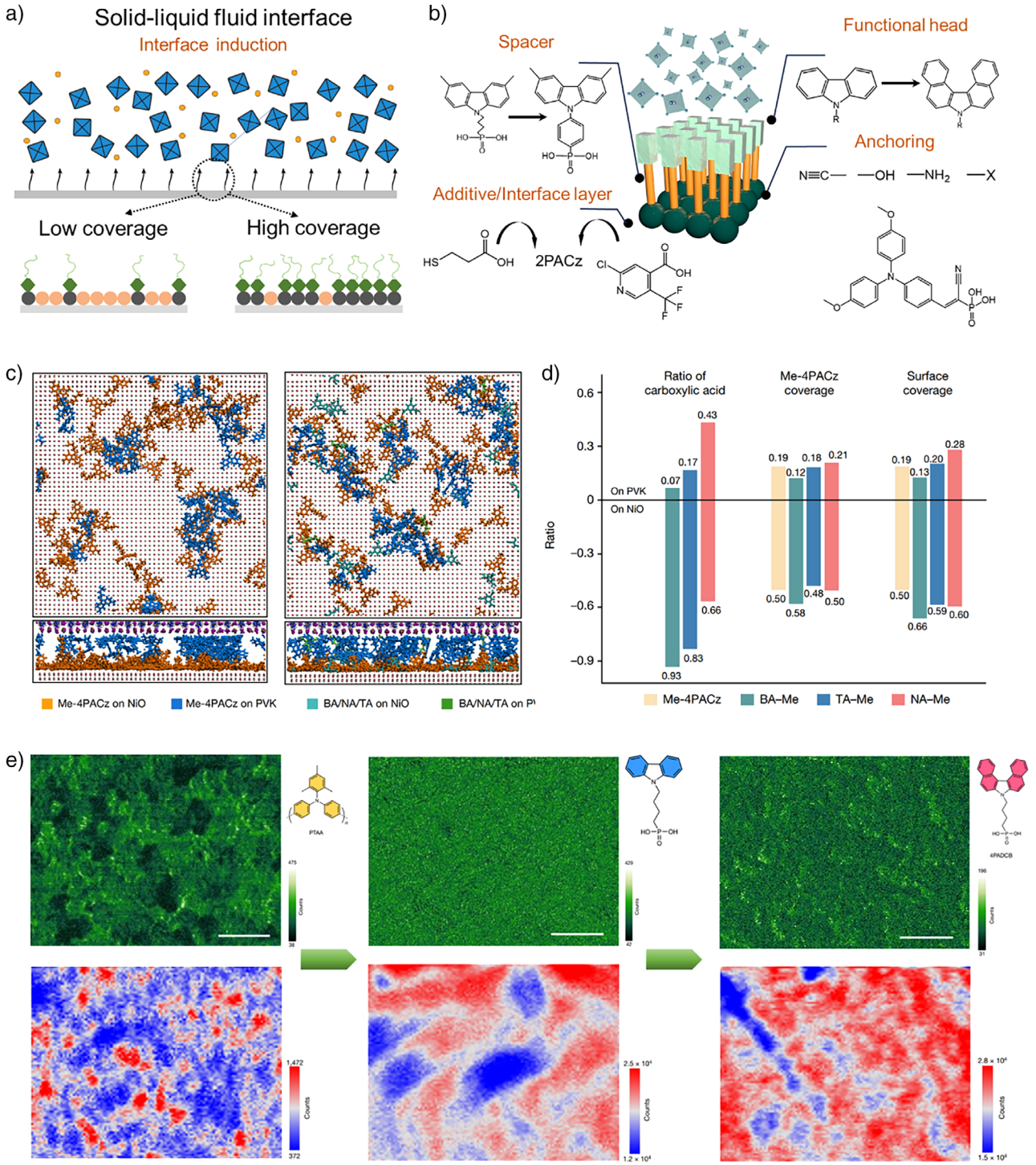

Figure 8. The chemistry reaction of the solid–liquid fluid interface. a) The solid–liquid fluid interface induced by bottom interface material. b) Four regulatory strategies for SAMs materials. c) Top and side views of equilibrated molecular representations of the heterojunctions Me-4PACz and NA-Me. d) Adsorption analysis of the perovskite and NiO surface in the heterojunction models for Me-4PACz, BA-Me, NA-Me, and TA-Me hybrids, c) and (d) adapted from Ref. [169] with permission. e) Molecular structure, electrostatic surface potential and the photo-induced surface potential mapping for PTAA, 4PACz, and 4PADCB, adapted from Ref. [170] with permission.

Me-4PACz are significantly enhanced, and the final certified perovskite module performance was 22.74%. As shown in Figure 8e, a SAM of 4PADCB functions as a HTL in wide-bandgap PSCs.[170] The improvement in film coverage and surface wettability is achieved by introducing a new terminal group of 7*H*-dibenzocarbazole (DCB), enabling high-efficient hole extraction. The 4PADCB sample exhibits the smallest amplitude of potential change and significantly reduced contact angle, suggesting a more uniform anchoring and improved wettability compared to PTAA and 4PACz,

attributed to the steric hindrance of the DCB terminal group. Finally, the PCE of 27.01% is achieved for all-perovskite TSCs.

The inherently poor mechanical properties of perovskite films, characterized by their compliance (low Young's modulus), softness (low hardness), and brittleness (low toughness), stem from the low formation energies involved in MHPs. I-SAM have been utilized to significantly enhance the adhesion toughness at the interface between the ETL and the halide perovskite film.[171] PSCs based on I-SAM are observed to exhibit minimal damage accumulation and enhanced device performance, which is attributed to a combination of reduced hydroxyl groups at the interface and increased interfacial toughness. To ensure better deposition quality of the SAMs and reduce interface recombination, a high-quality compact p-type NiO_x HTL is required. Recently, the dispersion of NiO_x nanoparticles (NPs) is improved by incorporating H_2O_2, preventing particle aggregation that could hinder full coverage of the transparent TCO substrate.[172]

4.2. Interfacial Chemistry of Intermediate Phase

4.2.1. Gas-Intermediate Phase Interface

The thermal evaporation deposition method facilitates the transition of perovskite raw material into gas fluid within enclosed space at elevated temperatures, enabling the deposition of perovskite film and the construction of heterostructure on the substrate.[173] For this solvent-free perovskite deposition method, regulating the gas-fluid evaporation process and the layer–layer structure of the mesophase films during the transition from gas fluid to intermediate phase are the main study directions of gas-intermediate phase interface (Figure 9a). At the interface between the Pb–Sn perovskite and the ETL, an immiscible 3D/3D bilayer perovskite heterojunction (PHJ) is employed to suppress interfacial non-radiative recombination and aid in charge extraction due to its type II band structure using a hybrid thermal evaporation-solution processing method.[157] Figure 9b illustrates the device architecture of mixed Pb–Sn PSCs with a bilayer PHJ constructed using only 3D perovskites, wherein a full-lead wide-bandgap (FL-WBG) perovskite layer is deposited on the top of mixed Pb–Sn perovskite utilizing a hybrid two-step method. The ToF-SIMs results reveal that Pb^{2+} and Sn^{2+} ions are evenly distributed within the Pb–Sn perovskite film, with a stronger signal of Pb^{2+} near the heterojunction surface (representing the FL-WBG layer) and no noticeable signal of Sn^{2+} (Figure 9c). The type II band alignment between the Pb–Sn and FL-WBG perovskites could reduce the hole concentration, which attribute to reduce charge recombination and facilitate electron extraction owing to the suitable band bending (Figure 9d). Consequently, a record-high PCE of 28.5% (certified 28.0%) is achieved in all-perovskite tandem solar cells (Figure 9e). The bottom interface of 2D/3D heterolayers have been less studied, mainly because the pre-deposited 2D layers are easily dissolved or washed out. The alkylamine ligand phosphonic acid ($-PO(OH)_2$) forms an ionic bond through the acid–base reaction with the phosphonic acid group of 2PACz, which strengthens the adhesion of $-PO(OH)_2$ to the substrate, thereby improving the formation of 2D perovskite materials.[174] Applying a two-step deposition method involving lead halide vapor treatment and cation spin-coating, this approach yields a stable, pure-phase 2D perovskite layer at the lower interface, resulting in 2D/3D PSCs with a certified efficiency of 25.0%.

4.2.2. Liquid-Intermediate Phase Interface

The crystallization and growth of perovskite films in a liquid environment, studied from a dynamic fluid perspective, is a novel and understudied research area (Figure 9a). Recent studies have demonstrated that liquid environment can retarding nucleation and promoting crystal growth of perovskite according to the LaMer model.[175–177] Due to local fluctuations in the processing atmosphere, poor perovskite films with low reproducibility can often be produced. Additionally, the loss of volatile components may result in coincident defects and substantial inhomogeneity across large-area films. To tackle these challenges, liquid medium annealing (LMA) technology has been introduced, creating a robust chemical environment and a constant heating field to uniformly modulate crystal growth across the film.[178] This approach results in perovskite films characterized by high crystallinity, minimal defects, desired stoichiometry, and enhanced homogeneity. As shown in Figure 9f, the heating mode for LMA analyzed through finite element analysis, simulates the thermal field and annealing times. The faster heating at the solid–liquid fluid interface allows immediate warming of the entire film attributed to the top–down heating mode, compared to the delayed heat transferring through glass and significant thermal convection between perovskite and air in the traditional approach. The LMA method demonstrates a significantly faster heating rate compared to the reference, attributed to stabilizing the thermal field on the perovskite films by mitigating unfavorable thermal convection with air (Figure 9g). Furthermore, the negligible thickness compared to the substrate allows a minimal temperature variation along its vertical direction, accelerating the diffusion of reactants such as organic cations and Pb-I octahedra, thereby fostering a higher grain growth rate. As shown in Figure 9h, PSCs utilizing LMA method achieves a PCE of 24.04%, maintaining 95% of their initial PCE after 2000 h, showing the potential of LMA in enhancing film quality and PSCs stability (Figure 9i).

5. Large-Area PSCs Based on Fluid Chemistry

The main challenge of industrialization of PSCs is the reproducible and low-cost preparation of perovskite films.[121,179] At present, the small-area PSCs with the highest certified efficiency are still prepared by spin-coating method. High-efficiency spin-coated perovskite devices are focused on by optimizing interface engineering, film morphology control, rapid nucleation and crystal growth, composition tuning, and

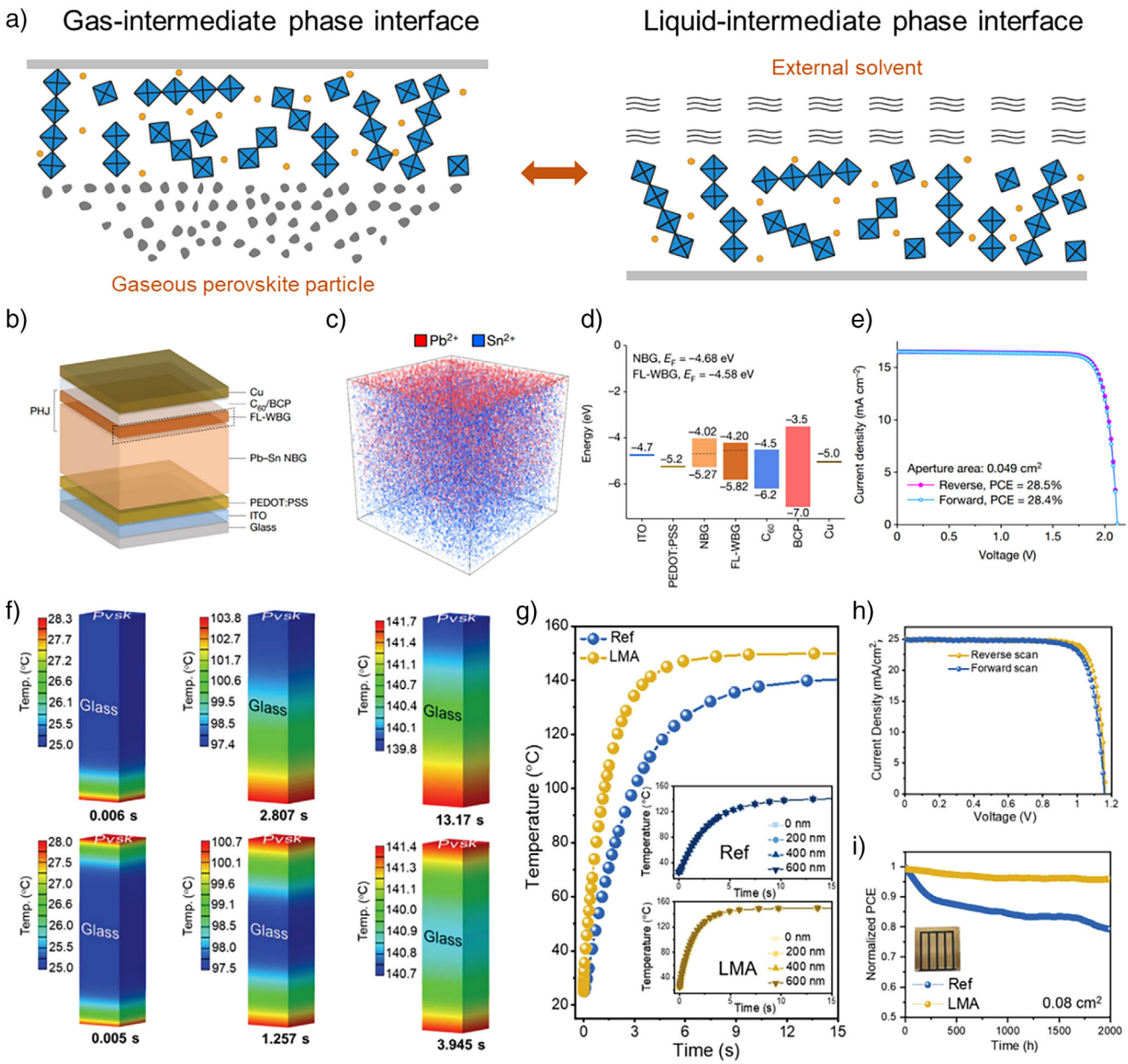

Figure 9. The chemistry reaction of the intermediate phase interface. a) The schematic diagram of the gas-intermediate phase interface during transition process by thermal evaporation and the liquid-intermediate phase interface induced by external liquid. b) The structure of Pb-Sn PSCs with a 3D/3D bilayer perovskite heterojunction. c) The ToF-SIMs distribution of Pb^{2+} and Sn^{2+} ions within perovskite films. d) Energy level of each layer in Pb–Sn PSCs with perovskite heterojunction. e) The performance of all-perovskite tandem solar cells with 3D/3D bilayer perovskite heterojunction in mixed Pb–Sn solar cell under reverse and forward scans, b–e) adapted from Ref. [157] with permission. f) Finite element analysis on the thermal field distribution with annealing time based on liquid medium annealing and traditional crystallization dynamics processes. g) The film evolution of surface temperature with annealing time. h) The *J–V* curves of liquid medium annealing perovskite devices with reverse scan and forward scan. i) The stability of PSCs based on LMA technology, f–i) adapted from Ref. [178] with permission.

stability enhancement.[180,181] However, with the increase of active layer area, the distribution of perovskite solution in the center and edge of the substrate is significantly different, which makes the spin-coating process not suitable for the preparation of large-area PSCs. Therefore, the study of perovskite crystallization by fluid chemistry theory mainly focuses on the preparation methods of large-area perovskite films. As shown in Figure 10a, the perovskite films can be prepared by gas-fluid or liquid-fluid film forming methods. Gas fluid deposition has distinct unidirectional deposition characteristics, including vapor deposition and spray coating. Thermal evaporation is an upward deposition method that enables the uniform preparation of large-area perovskite films with minimal material waste by precisely controlling the growth environment and rate of perovskite.[182–184] The movement process of perovskite gas fluids within the chamber determines the intermediate phase morphology and structure of thermally evaporated perovskite films, and the distribution

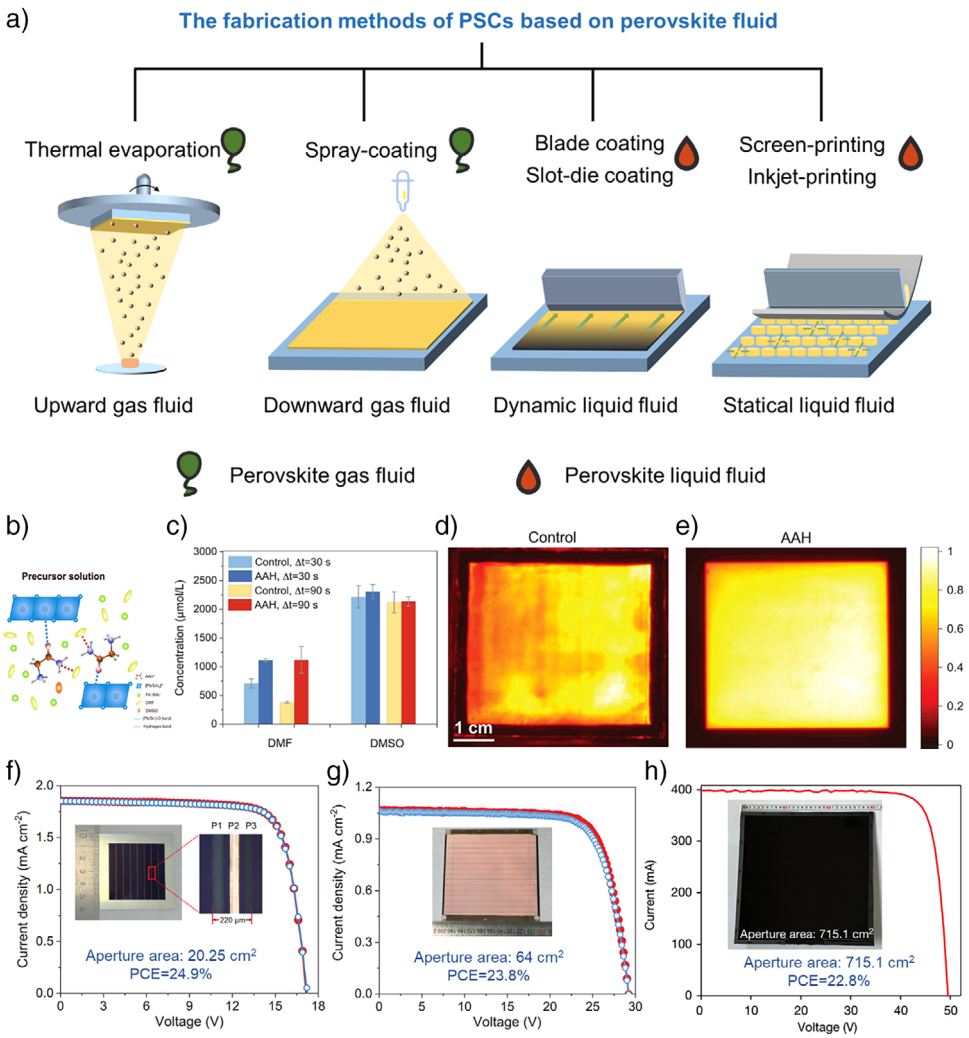

Figure 10. Large-area perovskite films and modules based on the liquid fluid and gas fluid. a) The mainstream fabrication methods of PSCs. The upward-deposition of perovskite gas fluid represented by thermal evaporation. The downward-deposition of perovskite gas fluid represented by spraying process. The following-deposition of dynamic perovskite liquid fluid represented by the coating methods. The spreading-deposition of statical perovskite liquid fluid represented by the printing methods. b) Schematic diagram of extending the processing window. c) Gas chromatography (GC) of the control and AAH blade-coated wet perovskite films with different delay times. PL mapping images of d) control and e) AAH samples. f) Photovoltaic performance of 20.25 cm^2 all-perovskite tandem solar cells with AAH. g) Photovoltaic performance of 64 cm^2 all-perovskite tandem solar cells with AAH, b–g) adapted from Ref. [198] with permission. h) *J–V* curve of the 30 × 30 cm^2 target perovskite module, adapted from Ref. [200] with permission.

uniformity of perovskite fluids on substrates can be achieved by controlling the size of perovskite crystals and the distance from the chamber.[183] Additionally, by designing the surface tension and adsorption properties between the underlying substrate and the gas fluid, the interaction strength and growth mode of perovskite materials on the substrate can be adjusted to suppressed crystal defects and film clusters.[48,60] Currently, thermal evaporation has been proven effective for preparing high-quality perovskite films, and mini perovskite modules based on vapor deposition have shown promising performance in laboratory.[184] We believe that precise control and measurement of the deposition rate and ratio of raw materials are crucial for vapor-deposited perovskite films to achieve accurate layer-by-layer evaporation and uniform distribution of gas fluids in a film. As MAI or FAI evaporates omnidirectionally, it is necessary to implement partial pressure monitoring of organic materials to enhance the accuracy of thermal evaporation. Moreover, for the chemical components of perovskite gas fluid, suitable halogen materials can extend the molecular diffusion distance and promote the deep reaction of perovskite fluid. In the future, it is still necessary to further improve its stability through transport layer screening and defect passivation. Compared with thermal evaporation, spray coating is a downward deposition method for large-area perovskite deposition, which can disperse perovskite solution into gas-like tiny liquids under the action of intracavitary pressure and deposit on various substrates.[185–187] In recent years, the PCE of PSCs based on the spray coating method has significantly lower than that of other fluid methods, due to the rapid crystallization

of the spray fluid during the printing process, resulting in increased defects and discontinuous films. Despite film quality and stability challenges, PSCs based on spray coating method can be enhanced by solvent coordination, additive chemistry, and interface materials.[188,189]

The deposition of perovskite liquid fluids can be classified into dynamic following and static spreading. The dynamic fluid deposition, represented by methods such as blade coating and slot-die coating, involves perovskite fluid following the movement of instrument in a fixed direction while undergoing deposition process under heating.[190–192] This method can typically yield perovskite films with high flatness, but the solvent evaporation during coating is unstable, potentially leading to more internal or surface defects.[193,194] Therefore, research primarily focuses on optimizing coating processes, chemical compositions, interface effects, solvent components, and additives. Currently, the perovskite modules have achieved a highest PCE of 23.30% over a 27.22 cm^2 aperture area for single-junction PSCs. Due to its controlled crystallization process and straightforward preparation, the blade coating method has emerged as a dependable technique for producing liquid-fluid perovskite films.[195–197] Owing to the heterogeneous crystallization and inferior buried interfaces. The aminoacetamide hydrochloride (AAH), a dopant from biochemical buffers, has been utilized to uniform crystallization, extended the processing window for blade-coating Pb–Sn perovskite films and passivated defects at buried interfaces.[198] As shown in Figure 10b, the interactions between AAH and almost all perovskite components are facilitated, including PbI_2, SnI_2, FAI, and solvent. As shown in Figure 10c, the Cl^- could delay crystallization and extend processing window for blade-coating, yielding a pinhole-free Pb–Sn perovskite thin film with vertically oriented grains. This improvement is also reflected in the photoluminescence (PL) mapping of the perovskite film (Figure 10d,e). As shown in Figure 10f,g, the all-perovskite TSCs achieving PCE of 24.9% (20.25 cm^2) and 23.8% (64 cm^2). Furthermore, the crystal nucleation rate of WBG perovskite film could be controlled by tuning the cesium ratio by a gas-assisted blade-coating method, improving the homogeneity of large-area films.[199] Traditional impurity repair strategies may hinder the deposition of subsequent materials, the functional cation 2-(1-cyclohexenyl)ethylammonium (CHEAI) was able to convert excess PbI_2 and δ-$FAPbI_3$ impurities into $CHEA_2PbI_4$ with high charge transport ability.[200] This also helps to improve the wettability and fluidity of the hole material. The module with an aperture area of 715.1 cm^2 achieved a record efficiency of 22.80% (Figure 10h).

Additionally, statical deposition of perovskite liquid fluid results in a series of vertically oriented and discontinuous perovskite dispersion droplets on the substrate, which can eventually form smooth wet films after a period of time, including screen-printing and inkjet-printing methods.[100,198,201–203] As the printing process of perovskite is usually separated from solvent annealing, there will inevitably be adverse CRE or wrinkling in the annealing process of wet perovskite film.[72,84] Therefore, the research direction on large-area perovskite films should focus on the transformation process from precursor to wet film, so as to improve the flatness of wet films and reduce defects of deposited films.[76] Priority selection should be given to considering solvent composition, viscosity control, surface chemistry, and developing advanced liquid fluid deposition processes to overcome these challenges.[73,204] Such as the highly viscous and deprotonated ionic liquid MAAc is used for the preparation of perovskite printing inks and for the preparation of 3D controllable screen-printed perovskite films and devices.[100] Currently, screen-printing is the primary method for producing silicon and dye-sensitized solar cells due to its simplicity and cost-effectiveness, enhancing industrial competitiveness.[204] However, traditional solvents are difficult to be applied to screen-printing perovskite films and devices due to low viscosity and poor stability. Our group discovers that ionic liquid perovskite inks offer high viscosity and stability due to electrostatic interaction between anions and cations, inhibiting irregular perovskite movement and improving ink chemistry stability.[100] Based on these perovskite inks with controllable viscosity and composition, we successfully prepared screen-printed perovskite films in arbitrary environmental conditions. Screen-printing method enables precise deposition of nanoscale perovskite films in three dimensions, overcoming issues like material waste and large-area uniformity associated with conventional methods. Further, the highest PCE of 20.52% (0.05 cm^2) and 18.12% (1 cm^2) regardless of humidity are achieved. Most importantly, we develop fully screen-printed PSCs using a single machine in ambient air. These devices maintain high PCE of 14.98%, 13.53%, and 11.80% on areas of 0.05, 1.00, and 16.37 cm^2, respectively.

6. Conclusions and Outlook

Thermodynamic parameters (annealing temperature, annealing time, etc.) and environmental conditions (humidity, oxygen content, etc.) are the basic conditions to determine whether perovskite can phase transition, and further fluid chemistry can more clearly describe the changes in the film and crystal during the phase transition process. Therefore, the fluid chemistry of MHPs has been extensively studied, leading to significant advancements in perovskite film quality and device performance. Despite this progress, significant opportunities for further development remain. In this review, we discuss the main fluid behaviors of MHPs, the internal crystallization chemistry, the external interfacial chemistry, and the large-area PSCs based on gas fluid and liquid fluid. We first introduce the basic fluid behaviors and the stability of perovskite materials. Then, we explore the solvent chemistry and additive engineering to further understand the crystal evolution and chemical interaction within perovskite ink. Subsequently, we focus on the interfacial chemistry of perovskite ink during crystallization by the introduction of gas-fluid and liquid-fluid, including four parts: I. gas–liquid fluid interface, II. solid–liquid fluid interface, III. gas-intermediate phase interface, and IV. liquid-intermediate phase interface. Finally, we summarize the fabrication methods of large-area perovskite film and device based on gas fluid methods and liquid fluid methods. The above research provides a deep understanding for fluid chemistry of MHPs.

Moreover, we outline four directions for future exploration aimed at addressing the constraints encountered by PSCs employing fluid chemistry theory. Primarily, there is an urgent imperative to foster a more profound understanding of the intricate fluid behavior and deposition process. At the microscopic point of view, perovskite fluid chemistry should focus on the deposition process of perovskite materials, aiming to from an ordered crystal structure, which is attributed to the ordered arrangement of chemical molecules in liquid fluid and the ordered perovskite crystallization and growth process. At present, most additives or passivators actually form coordination bonds or hydrogen bond networks with perovskite raw materials to achieve ordered intermediate phase, which is conducive to the ordered crystallization and growth of perovskite crystals. More critically, a "locally ordered" molecular arrangement is constructed directly inside the preliminary perovskite material to control the order degree of perovskite from the source. The "local order" of liquid fluid is mainly determined by ion–dipole interaction and electrostatic interaction, which is conducive to the design of local solvation structure, the chemical reaction dynamic process, the fluid ion transport behavior at the interface, the perovskite material energy level structure and the fluid diffusion and arrangement. It also determines the ordered crystallization process of perovskite materials. With the gradual integration of fluid chemistry theory in the phase transition process of perovskite, specific regulation strategies will emerge quickly in PSCs field. From a macro perspective, much of the research in this realm has leaned on a restricted array of surface-level characterization techniques, lacking a cohesive inquiry and definitive proof on the fluid motion process affected by various parameters. Therefore, it is imperative to carefully consider aspects such as the chemical interaction, motion resistance, fluid fluctuation, coupling effects, and seed floating between the fluid and the substrate to conceive the target fluid motion process comprehensively.

Second, we recommend employing high-throughput experimental techniques and machine learning algorithms to simulate the molecular motion and bonding within perovskite ink. This approach aims to identify suitable preparation processes, solvents, and additives, which is crucial for optimizing perovskite device performance. Currently, most results focus on one or several compounds, but the repeatability of experiments heavily depends on the experimental environment and operational details. This variability makes it challenging to directly compare results obtained by different research groups. Given the significant impact of fluid on the performance and stability of perovskite films and devices, machine learning or theoretical calculation offer effective method to further understand the complex and ongoing crystallization process experienced by MHPs. For example, Kirkwood–Buff (KB) theory is of great significance for the study of local aggregation and macroscopic thermodynamic quantities of complex fluids, which determine the properties of fluids and subsequent crystallization processes. KB theory can be used to predict the interaction of components in a fluid, describe the thermodynamic properties of mixed perovskite inks, including the conditions under which the liquid–liquid separation phenomenon and the phase equilibrium configuration, the heat value of the mixed perovskite inks based on the Kirkwood–Buff integral, and the compensation effect of perovskite solute-solution. Beyond Kirkwood–Buff theory, other theoretical approaches and computational models, such as molecular dynamics simulation (MDS), finite element method (FEM), Monte Carlo simulation (MCS), and lattice Boltzmann method (LBM), are under active development and hold promise for advancing theoretical understanding of MHP fluid chemistry.

Third, we assert the necessity for a more comprehensive exploration of fluid interfaces, as the rapid and intense chemical reactions undoubtedly originate at these interfaces before spreading into the crystals. For example, SAMs have demonstrated their advantages as bottom interface or HTL materials in improving perovskite crystallization and carrier transport in recent years, effectively advancing the theoretical basis of perovskite interface chemistry. At the same time, it should be recognized that the degradation of perovskite materials under adverse conditions often initiates at these interfaces. Environmental factors such as moisture, oxygen, and light, as well as chemical interactions with charge transport layers and electrode materials, can trigger interfacial reactions that lead to structural decomposition, ion migration, and device instability. Therefore, suppressing these complex interfacial chemical reactions is essential to enhancing the long-term operational stability of PSCs. Promising strategies include the introduction of appropriate additives into precursor solutions and the incorporation of buffer layers to modulate the fluid interface behavior during film formation. These approaches not only optimize the crystallization process but also create more stable interfaces that can resist environmental degradation.

Fourth, the issue of Pb toxicity remains a critical challenge that must be addressed to enable the large-scale commercialization of MHPs. Although Pb-free perovskite materials, including Sn^{2+}, Bi^{3+}, Sb^{3+}, and Ge^{2+}, have been extensively investigated, their practical application is significantly limited by inherent drawbacks, such as poor chemical stability, high susceptibility to oxidation, insufficient crystallization kinetics, and poor film quality, all of which hinder device performance and operational stability. To address these issues, fluid chemistry strategies offer effective and feasible solutions. By carefully optimizing the composition of precursor solutions and adjusting key fluid parameters such as polarity, viscosity, surface tension, diffusion, adhere behaviors, the crystallization process of Pb-free perovskite thin films can be precisely controlled, resulting in dense and highly crystalline perovskite films with enhanced intrinsic stability and device performance. Furthermore, fluid chemistry plays an important role in optimizing the fabrication of protective layers and buffer interfaces. Through precise control, the fluid properties and interfacial behavior during the deposition process, compact and uniform protective layers can be achieved. These layers effectively prevent the permeation of moisture and oxygen, thereby suppressing the environmental degradation of the perovskite layer and reducing the risk of Pb leakage. In

addition, recycling and recovery technologies guided by fluid chemistry principles, such as solvent-assisted selective extraction, offer practical approaches for the efficient recovery of Pb from perovskite devices.

Finally, considering fluid chemistry plays a fundamental role in the perovskite phase transition, it is imperative to extend the newly developed processes and perovskite materials to industrial production lines and test their theoretical feasibility. This initiative is crucial for fundamentally enhancing the commercial competitiveness of PSCs.

Acknowledgements

This work was financially supported by the Natural Science Foundation of China (22425903, U24A20568, 61705102, 62288102, 22409091, 22409090, and 62205142), the National Key R&D Program of China (2023YFB4204500 and 2020YFA07099003), the Jiangsu Provincial Departments of Science and Technology (BE2022023, BK20220010, BZ2023060, and BK20241875).

Conflict of Interests

The authors declare no conflict of interest.

Data Availability Statement

The data that support the findings of this study are available from the corresponding author upon reasonable request.

Keywords: Fluid behavior · Fluid chemistry · Fluid stability · Interfacial chemistry · Large-area module

[1] A. Kojima, K. Teshima, Y. Shirai, T. Miyasaka, *J. Am. Chem. Soc.* **2009**, *131*, 6050–6051.
[2] D. T. Moore, H. Sai, K. W. Tan, D.-M. Smilgies, W. Zhang, H. J. Snaith, U. Wiesner, L. A. Estroff, *J. Am. Chem. Soc.* **2015**, *137*, 2350–2358.
[3] J. J. Yoo, G. Seo, M. R. Chua, T. G. Park, Y. Lu, F. Rotermund, Y.-K. Kim, C. S. Moon, N. J. Jeon, J.-P. Correa-Baena, V. Bulović, S. S. Shin, M. G. Bawendi, J. Seo, *Nature* **2021**, *590*, 587–593.
[4] S. Tao, I. Schmidt, G. Brocks, J. Jiang, I. Tranca, K. Meerholz, S. Olthof, *Nat. Commun.* **2019**, *10*, 2560.
[5] M. Y. Wei, F. P. G. de Arguer, G. Walters, Z. Y. Yang, L. N. Quan, Y. Kim, R. Sabatini, R. Quintero-Bermudez, L. Gao, J. Z. Fan, F. J. Fan, A. Gold-Parker, M. F. Toney, E. H. Sargent, *Nat. Energy* **2019**, *4*, 197–205.
[6] Q. A. Akkerman, V. D'Innocenzo, S. Accornero, A. Scarpellini, A. Petrozza, M. Prato, L. Manna, *J. Am. Chem. Soc.* **2015**, *137*, 10276–10281.
[7] J. Huang, Y. Yuan, Y. Shao, Y. Yan, *Nat. Rev. Mater.* **2017**, *2*, 17042.
[8] A. Al-Ashouri, E. Köhnen, B. Li, A. Magomedov, H. Hempel, P. Caprioglio, J. A. Márquez, A. B. M. Vilches, E. Kasparavicius, J. A. Smith, N. Phung, D. Menzel, M. Grischek, L. Kegelmann, D. Skroblin, C. Gollwitzer, T. Malinauskas, M. Jost, G. Matic, B. Rech, R. Schlatmann, M. Topic, L. Korte, A. Abate, B. Stannowski, D. Neher, M. Stolterfoht, T. Unold, V. Getautis, S. Albrecht, *Science* **2020**, *370*, 1300–1309.
[9] Z. Ni, C. Bao, Y. Liu, Q. Jiang, W.-Q. Wu, S. Chen, X. Dai, B. Chen, B. Hartweg, Z. Yu, Z. Holman, J. Huang, *Science* **2020**, *367*, 1352–1358.
[10] R. Wang, J. Xue, K.-L. Wang, Z.-K. Wang, Y. Luo, D. Fenning, G. Xu, S. Nuryyeva, T. Huang, Y. Zhao, J. L. Yang, J. Zhu, M. Wang, S. Tan, I. Yavuz, K. N. Houk, Y. Yang, *Science* **2019**, *366*, 1509–1513.
[11] Y. Yang, J. B. You, *Nature* **2017**, *544*, 155–156.
[12] F. Gao, Y. Zhao, X. W. Zhang, J. B. You, *Adv. Energy Mater.* **2020**, *10*, 1902650.
[13] M. He, B. Li, X. Cui, B. B. Jiang, Y. J. He, Y. H. Chen, D. O'Neil, P. Szymanski, M. A. El-Sayed, J. S. Huang, Z. Q. Lin, *Nat. Commun.* **2017**, *8*, 16045.
[14] Q. Hu, L. C. Zhao, J. Wu, K. Gao, D. Y. Luo, Y. F. Jiang, Z. Y. Zhang, C. H. Zhu, E. Schaible, A. Hexemer, C. Wang, Y. Liu, W. Zhang, M. Grätzel, F. Liu, T. P. Russell, R. Zhu, Q. H. Gong, *Nat. Commun.* **2017**, *8*, 15688.
[15] M. J. Yang, Z. Li, M. O. Reese, O. G. Reid, D. H. Kim, S. Siol, T. R. Klein, Y. Yan, J. J. Berry, M. van Hest, K. Zhu, *Nat. Energy* **2017**, *2*, 17038.
[16] P. W. Liang, C. Y. Liao, C. C. Chueh, F. Zuo, S. T. Williams, X. K. Xin, J. J. Lin, A. K. Y. Jen, *Adv. Mater.* **2014**, *26*, 3748–3754.
[17] Y. H. Deng, X. P. Zheng, Y. Bai, Q. Wang, J. J. Zhao, J. S. Huang, *Nat. Energy* **2018**, *3*, 560–566.
[18] Q. Wang, Q. F. Dong, T. Li, A. Gruverman, J. S. Huang, *Adv. Mater.* **2016**, *28*, 6734–6739.
[19] K. Y. Yan, M. Z. Long, T. K. Zhang, Z. H. Wei, H. N. Chen, S. H. Yang, J. B. Xu, *J. Am. Chem. Soc.* **2015**, *137*, 4460–4468.
[20] S. Tan, T. Y. Huang, I. Yavuz, R. Wang, M. H. Weber, Y. P. Zhao, M. Abdelsamie, M. E. Liao, H. C. Wang, K. Huynh, K. H. Wei, J. J. Xue, F. Babbe, M. S. Goorsky, J. W. Lee, C. M. Sutter-Fella, Y. Yang, *J. Am. Chem. Soc.* **2021**, *143*, 6781–6786.
[21] W. Zhang, M. Saliba, D. T. Moore, S. K. Pathak, M. T. Hörantner, T. Stergiopoulos, S. D. Stranks, G. E. Eperon, J. A. Alexander-Webber, A. Abate, A. Sadhanala, S. H. Yao, Y. L. Chen, R. H. Friend, L. A. Estroff, U. Wiesner, H. J. Snaith, *Nat. Commun.* **2015**, *6*, 6142.
[22] Y. P. Zhao, P. C. Zhu, S. Huang, S. Tan, M. H. Wang, R. Wang, J. J. Xue, T. H. Han, S. J. Lee, A. N. Zhang, T. Y. Huang, P. Cheng, D. Meng, J. W. Lee, J. Marian, J. Zhu, Y. Yang, *J. Am. Chem. Soc.* **2020**, *142*, 20071–20079.
[23] Z. Q. Li, X. Y. Liu, C. L. Zuo, W. Yang, X. S. Fang, *Adv. Mater.* **2021**, *33*, 2103010.
[24] Z. M. Zhou, Z. W. Wang, Y. Y. Zhou, S. P. Pang, D. Wang, H. X. Xu, Z. H. Liu, N. P. Padture, G. L. Cui, *Angew. Chem. Int. Ed.* **2015**, *54*, 9705–9709.
[25] H. Y. Dong, C. H. Zhang, X. L. Liu, J. N. Yao, Y. S. Zhao, *Chem. Soc. Rev.* **2020**, *49*, 951–982.
[26] M. Jung, S. G. Ji, G. Kim, S. I. Seok, *Chem. Soc. Rev.* **2019**, *48*, 2011–2038.
[27] Z. Huang, Y. Bai, X. Huang, J. Li, Y. Wu, Y. Chen, K. Li, X. Niu, N. Li, G. Liu, Y. Zhang, H. Zai, Q. Chen, T. Lei, L. Wang, H. Zhou, *Nature* **2023**, *623*, 531–537.
[28] Y. Deng, X. Zheng, Y. Bai, Q. Wang, J. Zhao, J. Huang, *Nat. Energy* **2018**, *3*, 560–566.
[29] P. Zhu, D. Wang, Y. Zhang, Z. Liang, J. Li, J. Zeng, J. Zhang, Y. Xu, S. Wu, Z. Liu, X. Zhou, B. Hu, F. He, L. Zhang, X. Pan, X. Wang, N.-G. Park, B. Xu, *Science* **2024**, *383*, 524–531.
[30] S. Zhang, F. Ye, X. Wang, R. Chen, H. Zhang, L. Zhan, X. Jiang, Y. Li, X. Ji, S. Liu, M. Yu, F. Yu, Y. Zhang, R. Wu, Z. Liu, Z. Ning, D. Neher, L. Han, Y. Lin, H. Tian, W. Chen, M. Stolterfoht, L. Zhang, W.-H. Zhu, Y. Wu, *Science* **2023**, *380*, 404–409.
[31] A. K. Jena, A. Kulkarni, T. Miyasaka, *Chem. Rev.* **2019**, *119*, 3036–3103.

[32] F. H. Isikgor, S. Zhumagali, L. V. T. Merino, M. De Bastiani, I. McCulloch, S. De Wolf, *Nat. Rev. Mater.* **2023**, *8*, 89–108.
[33] F. Tian, L. L. Cai, C. Liu, J. S. Sun, *Lab Chip* **2022**, *22*, 512–529.
[34] E. Gong, S. Ali, C. B. Hiragond, H. S. Kim, N. S. Powar, D. Kim, H. Kim, S. I. In, *Energy Environ. Sci.* **2022**, *15*, 880–937.
[35] N. Fiuza-Maneiro, K. Sun, I. Lopez-Fernandez, S. Gomez-Grana, P. Muller-Buschbaum, L. Polavarapu, *ACS Energy Lett.* **2023**, *8*, 1152–1191.
[36] F. P. G. de Arquer, A. Armin, P. Meredith, E. H. Sargent, *Nat. Rev. Mater.* **2017**, *2*, 16100.
[37] H. Min, D. Lee, J. Kim, G. Kim, K. S. Lee, J. Kim, M. J. Paik, Y. K. Kim, K. S. Kim, M. G. Kim, T. J. Shin, S. I. Seok, *Nature* **2021**, *598*, 444–450.
[38] Q. Jiang, J. H. Tong, Y. M. Xian, R. A. Kerner, S. P. Dunfield, C. X. Xiao, R. A. Scheidt, D. Kuciauskas, X. M. Wang, M. P. Hautzinger, R. Tirawat, M. C. Beard, D. P. Fenning, J. J. Berry, B. W. Larson, Y. F. Yan, K. Zhu, *Nature* **2022**, *611*, 278–283.
[39] W. W. Zuo, M. M. Byranvand, T. Kodalle, M. Zohdi, J. Lim, B. Carlsen, T. M. Friedlmeier, M. Kot, C. Das, J. I. Flege, W. S. Zong, A. Abate, C. M. Sutter-Fella, M. Li, M. Saliba, *Adv. Mater.* **2023**, *35*, 2302889.
[40] H. P. Zhou, Q. Chen, G. Li, S. Luo, T. B. Song, H. S. Duan, Z. R. Hong, J. B. You, Y. S. Liu, Y. Yang, *Science* **2014**, *345*, 542–546.
[41] X. Lv, G. Y. Chen, X. Zhu, J. K. An, J. C. Bao, X. X. Xu, *Nano Res.* **2022**, *15*, 7590–7596.
[42] X. C. Li, Y. Meng, W. P. Li, J. Zhang, C. Q. Dang, H. Y. Wang, S. W. Hung, R. Fan, F. R. Chen, S. J. Zhao, J. C. Ho, Y. Lu, *Nat. Mater.* **2023**, *22*, 1175–1181.
[43] K. Sun, Z. Wang, N. Li, L. Liu, W. Xiong, Z. Xu, Z. Geng, X. Guo, Y. Jiang, S.-P. Feng, X. Gao, Y. Chen, J. Liu, J. Gao, *Adv. Mater.* **2025**, *37*, 2419419.
[44] W. Lv, Z. Hu, W. Qiu, D. Yan, M. Li, A. Mei, L. Xu, R. Chen, *Adv. Sci.* **2022**, *9*, 2202028.
[45] K. Xiao, R. X. Lin, Q. L. Han, Y. Hou, Z. Y. Qin, H. T. Nguyen, J. Wen, M. Y. Wei, V. Yeddu, M. I. Saidaminov, Y. Gao, X. Luo, Y. R. Wang, H. Gao, C. F. Zhang, J. Xu, J. Zhu, E. H. Sargent, H. R. Tan, *Nat. Energy* **2020**, *5*, 870–880.
[46] W. Peng, K. T. Mao, F. C. Cai, H. G. Meng, Z. J. Zhu, T. Q. Li, S. J. Yuan, Z. J. Xu, X. Y. Feng, J. H. Xu, M. D. McGehee, J. X. Xu, *Science* **2023**, *379*, 683–690.
[47] X. Jiang, B. Zhang, G. Yang, Z. Zhou, X. Guo, F. Zhang, S. Yu, S. Liu, S. Pang, *Angew. Chem. Int. Ed.* **2023**, *62*, e202302462.
[48] J. Xu, H. Chen, L. Grater, C. Liu, Y. Yang, S. Teale, A. Maxwell, S. Mahesh, H. Y. Wan, Y. X. Chang, B. Chen, B. Rehl, S. M. Park, M. G. Kanatzidis, E. H. Sargent, *Nat. Mater.* **2023**, *22*, 1507–1514.
[49] J. Zhu, Y. Luo, R. He, C. Chen, Y. Wang, J. Luo, Z. Yi, J. Thiesbrummel, C. Wang, F. Lang, H. Lai, Y. Xu, J. Wang, Z. Zhang, W. Liang, G. Cui, S. Ren, X. Hao, H. Huang, Y. Wang, F. Yao, Q. Lin, L. Wu, J. Zhang, M. Stolterfoht, F. Fu, D. Zhao, *Nat. Energy* **2023**, *8*, 714–724.
[50] J. Yi, J. Zhuang, X. C. Liu, H. Y. Wang, Z. Ma, D. J. Huang, Z. L. Guo, H. M. Li, *J. Alloys Compd.* **2020**, *830*, 154710.
[51] M. Liu, L. Y. Bi, W. L. Jiang, Z. X. Zeng, S. W. Tsang, F. R. Lin, A. K. Y. Jen, *Adv. Mater.* **2023**, *35*, 2304415.
[52] C. M. Wolff, L. Canil, C. Rehermann, N. Ngoc Linh, F. Zu, M. Ralaiarisoa, P. Caprioglio, L. Fiedler, M. Stolterfoht, S. Kogikoski, Jr., I. Bald, N. Koch, E. L. Unger, T. Dittrich, A. Abate, D. Neher, *ACS Nano* **2020**, *14*, 1445–1456.
[53] P. Tockhorn, J. Sutter, A. Cruz, P. Wagner, K. Jäger, D. Yoo, F. Lang, M. Grischek, B. Li, J. Li, O. Shargaieva, E. Unger, A. Al-Ashouri, E. Köhnen, M. Stolterfoht, D. Neher, R. Schlatmann, B. Rech, B. Stannowski, S. Albrecht, C. Becker, *Nat. Nanotechnol.* **2022**, *17*, 1214–1221.
[54] H. Li, J. Shi, J. Deng, Z. Chen, Y. Li, W. Zhao, J. Wu, H. Wu, Y. Luo, D. Li, Q. Meng, *Adv. Mater.* **2020**, *32*, 1907396.
[55] J. Qiu, X. Mei, M. Zhang, G. Wang, S. Zou, L. Wen, J. Huang, Y. Hua, X. Zhang, *Angew. Chem. Int. Ed.* **2024**, *63*, e202401751.
[56] A. Azimi Yancheshme, G. R. Palmese, N. J. Alvarez, *J. Colloid Interface Sci.* **2023**, *636*, 677–688.
[57] X. Wu, D. Gao, X. Sun, S. Zhang, Q. Wang, B. Li, Z. Li, M. Qin, X. Jiang, C. Zhang, Z. Li, X. Lu, N. Li, S. Xiao, X. Zhong, S. Yang, Z. Li, Z. Zhu, *Adv. Mater.* **2023**, *35*, 2208431.
[58] X. Wang, Z. Ying, J. Zheng, X. Li, Z. Zhang, C. Xiao, Y. Chen, M. Wu, Z. Yang, J. Sun, J.-R. Xu, J. Sheng, Y. Zeng, X. Yang, G. Xing, J. Ye, *Nat. Commun.* **2023**, *14*, 2166.
[59] Y. Ren, K. Zhang, Z. Lin, X. Wei, M. Xu, X. Huang, H. Chen, S. Yang, *Nano-Micro. Lett.* **2023**, *15*, 182.
[60] Y. Zhang, L. Ren, P. Zhai, J. Xin, J. Wu, Q. Zhang, X. Chen, K. Zhao, L. Zhang, S. Liu, *Energy Environ. Sci.* **2024**, *17*, 296–306.
[61] A. Al-Ashouri, E. Köhnen, B. Li, A. Magomedov, H. Hempel, P. Caprioglio, J. A. Márquez, A. B. Morales Vilches, E. Kasparavicius, J. A. Smith, N. Phung, D. Menzel, M. Grischek, L. Kegelmann, D. Skroblin, C. Gollwitzer, T. Malinauskas, M. Jošt, G. Matič, B. Rech, R. Schlatmann, M. Topič, L. Korte, A. Abate, B. Stannowski, D. Neher, M. Stolterfoht, T. Unold, V. Getautis, S. Albrecht, *Science* **2020**, *370*, 1300–1309.
[62] Y. Yao, C. Cheng, C. Zhang, H. Hu, K. Wang, S. De Wolf, *Adv. Mater.* **2022**, *34*, 2203794.
[63] T. H. Wu, L. K. Ono, R. Yoshioka, C. F. Ding, C. Y. Zhang, S. Mariotti, J. H. Zhang, K. Mitrofanov, X. Liu, H. Segawa, R. Kabe, L. Y. Han, Y. B. Qi, *Energy Environ. Sci.* **2022**, *15*, 4612–4624.
[64] M. He, B. Li, X. Cui, B. Jiang, Y. He, Y. Chen, D. O'Neil, P. Szymanski, M. A. Ei-Sayed, J. Huang, Z. Lin, *Nat. Commun.* **2017**, *8*, 16045.
[65] K. Liu, Q. Liang, M. Qin, D. Shen, H. Yin, Z. Ren, Y. Zhang, H. Zhang, P. W. K. Fong, Z. Wu, J. Huang, J. Hao, Z. Zheng, S. K. So, C.-S. Lee, X. Lu, G. Li, *Joule* **2020**, *4*, 2404–2425.
[66] C. Gong, B. Fan, F. Li, Z. Xing, X. Meng, T. Hu, X. Hu, Y. Chen, *Energy Environ. Sci.* **2022**, *15*, 4313–4322.
[67] J. Qi, S. Chen, C. Lan, A. C. Wang, X. Cui, Z. You, Q. Zhang, Y. Li, Z. L. Wang, H. Wang, Z. Lin, *Adv. Energy Mater.* **2020**, *10*, 2001185.
[68] X. Dai, Y. Deng, C. H. Van Brackle, J. Huang, *Int. J. Extreme Manuf.* **2019**, *1*, 022004.
[69] G. Shi, Z. Huang, R. Qiao, W. Chen, Z. Li, Y. Li, K. Mu, T. Si, Z. Xiao, *Nat. Commun.* **2024**, *15*, 1066.
[70] A. Kulkarni, R. Sarkar, S. Akel, M. Häser, B. Klingebiel, M. Wuttig, S. Wiegand, S. Chakraborty, M. Saliba, T. Kirchartz, *Adv. Funct. Mater.* **2023**, *33*, 2305812.
[71] C. Wei, W. Su, J. Li, B. Xu, Q. Shan, Y. Wu, Z. Fengjuan, M. Luo, H. Xiang, Z. Cui, H. Zeng, *Adv. Mater.* **2022**, *34*, 2107798.
[72] B. Fan, J. Xiong, Y. Zhang, C. Gong, F. Li, X. Meng, X. Hu, Z. Yuan, F. Wang, Y. Chen, *Adv. Mater.* **2022**, *34*, 2201840.
[73] H. Liu, G. Shi, R. Khan, S. Chu, Z. Huang, T. Shi, H. Sun, Y. Li, H. Zhou, P. Xiao, T. Chen, Z. Xiao, *Adv. Mater.* **2024**, *36*, 2309921.
[74] F. Yang, Q. Zeng, W. Dong, C. Kang, Z. Qu, Y. Zhao, H. Wei, W. Zheng, X. Zhang, B. Yang, *Light Sci. Appl.* **2023**, *12*, 119.
[75] L. Yuan, X. Chen, X. Guo, S. Huang, X. Wu, Y. Shen, H. Gu, Y. Chen, G. Zeng, H.-J. Egelhaaf, C. J. Brabec, F. Yang, Y. Li, Y. Li, *Angew. Chem. Int. Ed.* **2024**, *63*, e202316954.
[76] K. A. Bush, N. Rolston, A. Gold-Parker, S. Manzoor, J. Hausele, Z. J. Yu, J. A. Raiford, R. Cheacharoen, Z. C. Holman, M. F. Toney, R. H. Dauskardt, M. D. McGehee, *ACS Energy Lett.* **2018**, *3*, 1225–1232.
[77] Q. Du, C. Zhu, Z. Yin, G. Na, C. Cheng, Y. Han, N. Liu, X. Niu, H. Zhou, H. Chen, L. Zhang, S. Jin, Q. Chen, *ACS Nano* **2020**, *14*, 5806–5817.
[78] D. Bi, X. Li, J. V. Milić, D. J. Kubicki, N. Pellet, J. Luo, T. LaGrange, P. Mettraux, L. Emsley, S. M. Zakeeruddin, M. Grätzel, *Nat. Commun.* **2018**, *9*, 4482.

[79] J. Werner, T. Moot, T. A. Gossett, I. E. Gould, A. F. Palmstrom, E. J. Wolf, C. C. Boyd, M. F. A. M. van Hest, J. M. Luther, J. J. Berry, M. D. McGehee, *ACS Energy Lett.* **2020**, *5*, 1215–1223.

[80] B. Guo, M. Chauhan, N. R. Woodward, G. R. McAndrews, G. J. Thapa, B. M. Lefler, R. Li, T. Wang, K. Darabi, M. D. McGehee, A. Amassian, *ACS Energy Lett.* **2024**, *9*, 75–84.

[81] G. Li, Z. Su, L. Canil, D. Hughes, M. H. Aldamasy, J. Dagar, S. Trofimov, L. Wang, W. Zuo, J. J. Jerónimo-Rendon, M. M. Byranvand, C. Wang, R. Zhu, Z. Zhang, F. Yang, G. Nasti, B. Naydenov, W. C. Tsoi, Z. Li, X. Gao, Z. Wang, Y. Jia, E. Unger, M. Saliba, M. Li, A. Abate, *Science* **2023**, *379*, 399–403.

[82] M. Hu, Y. Zhu, Z. Zhou, M. Hao, C. Harnmanasvate, J. Waiyawat, Y. Wang, J. Lu, Q. An, X. Li, T. Zhang, Y. Zhou, R. Cheacharoen, Y. Rong, *Adv. Energy Mater.* **2023**, *13*, 2301888.

[83] Y. Zhao, F. Ma, Z. Qu, S. Yu, T. Shen, H.-X. Deng, X. Chu, X. Peng, Y. Yuan, X. Zhang, J. You, *Science* **2022**, *377*, 531–534.

[84] S.-G. Kim, J.-H. Kim, P. Ramming, Y. Zhong, K. Schötz, S. J. Kwon, S. Huettner, F. Panzer, N.-G. Park, *Nat. Commun.* **2021**, *12*, 1554.

[85] D.-J. Xue, Y. Hou, S.-C. Liu, M. Wei, B. Chen, Z. Huang, Z. Li, B. Sun, A. H. Proppe, Y. Dong, M. I. Saidaminov, S. O. Kelley, J.-S. Hu, E. H. Sargent, *Nat. Commun.* **2020**, *11*, 1514.

[86] J. Ye, D. Gaur, C. Mi, Z. Chen, I. L. Fernández, H. Zhao, Y. Dong, L. Polavarapu, R. L. Z. Hoye, *Chem. Soc. Rev.* **2024**, *53*, 8095–8122.

[87] R. Cheng, Z.-B. Liang, L. Zhu, H. Li, Y. Zhang, C.-F. Wang, S. Chen, *Angew. Chem. Int. Ed.* **2022**, *61*, e202204371.

[88] R. W. Epps, K. C. Felton, C. W. Coley, M. Abolhasani, *Lab Chip* **2017**, *17*, 4040–4047.

[89] P. Jha, N. Mukhin, A. Ghorai, H. Morshedian, R. B. Canty, F. Delgado-Licona, E. E. Brown, A. J. Pyrch, F. N. Castellano, M. Abolhasani, *Adv. Mater.* **2025**, 2419668.

[90] R. Cheng, Z.-B. Liang, H. Shen, J. Guo, C.-F. Wang, S. Chen, *Chinese Chem. Lett.* **2023**, *34*, 107384.

[91] I. Lignos, R. Maceiczyk, A. J. deMello, *Acc. Chem. Res.* **2017**, *50*, 1248–1257.

[92] T. Dong, J. Zhao, G. Li, F.-C. Li, Q. Li, S. Chen, *ACS Appl. Mater. Interfaces* **2021**, *13*, 39748–39754.

[93] Y. Geng, H. Hu, Y. Jia, X. Huang, T. Yang, R. Liang, Z. Chen, Z. Yuan, J. Xu, *Small Methods* **2023**, *7*, 2300394.

[94] J.-J. Li, T. Cui, J. Yu, Z.-B. Liang, Y. Liang, J. Li, S. Chen, *Nanoscale* **2022**, *14*, 11998–12006.

[95] X. Wang, Y. Fan, L. Wang, C. Chen, Z. Li, R. Liu, H. Meng, Z. Shao, X. Du, H. Zhang, G. Cui, S. Pang, *Chem* **2020**, *6*, 1369–1378.

[96] X. Liu, D. Luo, Z.-H. Lu, J. S. Yun, M. Saliba, S. I. Seok, W. Zhang, *Nat. Rev. Chem.* **2023**, *7*, 462–479.

[97] M. Wang, Z. Shi, C. Fei, Z. J. D. Deng, G. Yang, S. P. Dunfield, D. P. Fenning, J. Huang, *Nat. Energy* **2023**, *8*, 1229–1239.

[98] H. Min, G. Kim, M. J. Paik, S. Lee, W. S. Yang, M. Jung, S. I. Seok, *Adv. Energy Mater.* **2019**, *9*, 1803476.

[99] J. Zeng, X. Sun, Y. Liu, W. Jin, S. He, X. Zhu, K. Niu, G. Sun, J. Li, H. He, T. Sun, Z. Ye, Y. Jin, *Nat. Photon.* **2024**, *18*, 325–333.

[100] C. Chen, J. Chen, H. Han, L. Chao, J. Hu, T. Niu, H. Dong, S. Yang, Y. Xia, Y. Chen, W. Huang, *Nature* **2022**, *612*, 266–271.

[101] Y. Zou, W. Yu, H. Guo, Q. Li, X. Li, L. Li, Y. Liu, H. Wang, Z. Tang, S. Yang, Y. Chen, B. Qu, Y. Gao, Z. Chen, S. Wang, D. Zhang, Y. Chen, Q. Chen, S. M. Zakeeruddin, Y. Peng, H. Zhou, Q. Gong, M. Wei, M. Grätzel, L. Xiao, *Science* **2024**, *385*, 161–167.

[102] G. S. Shin, Y. Zhang, N.-G. Park, *ACS Appl. Mater. Interfaces* **2020**, *12*, 15167–15174.

[103] M. Yang, Z. Li, M. O. Reese, O. G. Reid, D. H. Kim, S. Siol, T. R. Klein, Y. Yan, J. J. Berry, M. F. A. M. van Hest, K. Zhu, *Nat. Energy* **2017**, *2*, 17038.

[104] L. Chen, M. Hu, A. M. Risqi, E. Noh, Y. Lee, S. I. Seok, *J. Am. Chem. Soc.* **2024**, *146*, 10159–10166.

[105] Y. Miao, M. Ren, Y. Chen, H. Wang, H. Chen, X. Liu, T. Wang, Y. Zhao, *Nat. Sustain.* **2023**, *6*, 1465–1473.

[106] N.-G. Park, *Nat. Sustain.* **2021**, *4*, 192–193.

[107] Y. Zhang, Z. Xing, B. Fan, Z. Ni, F. Wang, X. Hu, Y. Chen, *Angew. Chem. Int. Ed.* **2023**, *62*, e202215799.

[108] K. Wang, C. Wu, Y. Hou, D. Yang, W. Li, G. Deng, Y. Jiang, S. Priya, *Joule* **2020**, *4*, 615–630.

[109] H. Li, N. Shen, S. Chen, F. Guo, B. Xu, *Adv. Funct. Mater.* **2023**, *33*, 2214339.

[110] Y. Gao, H. Raza, Z. Zhang, W. Chen, Z. Liu, *Adv. Funct. Mater.* **2023**, *33*, 2215171.

[111] B.-w. Park, N. Kedem, M. Kulbak, D. Y. Lee, W. S. Yang, N. J. Jeon, J. Seo, G. Kim, K. J. Kim, T. J. Shin, G. Hodes, D. Cahen, S. I. Seok, *Nat. Commun.* **2018**, *9*, 3301.

[112] W. Hui, L. F. Chao, H. Lu, F. Xia, Q. Wei, Z. H. Su, T. T. Niu, L. Tao, B. Du, D. L. Li, Y. Wang, H. Dong, S. W. Zuo, B. X. Li, W. Shi, X. Q. Ran, P. Li, H. Zhang, Z. B. Wu, C. X. Ran, L. Song, G. C. Xing, X. Y. Gao, J. Zhang, Y. D. Xia, Y. H. Chen, W. Huang, *Science* **2021**, *371*, 1359–1364.

[113] T. L. Greaves, C. J. Drummond, *Chem. Rev.* **2008**, *108*, 206–237.

[114] K. L. Gardner, J. G. Tait, T. Merckx, W. Qiu, U. W. Paetzold, L. Kootstra, M. Jaysankar, R. Gehlhaar, D. Cheyns, P. Heremans, J. Poortmans, *Adv. Energy Mater.* **2016**, *6*, 1600386.

[115] H. Aqoma, S.-H. Lee, I. F. Imran, J.-H. Hwang, S.-H. Lee, S.-Y. Jang, *Nat. Energy* **2024**, *9*, 324–332.

[116] Y. Lin, Y. Fang, J. Zhao, Y. Shao, S. J. Stuard, M. M. Nahid, H. Ade, Q. Wang, J. E. Shield, N. Zhou, A. M. Moran, J. Huang, *Nat. Commun.* **2019**, *10*, 1008.

[117] N. K. Noel, B. Wenger, S. N. Habisreutinger, H. J. Snaith, *ACS Energy Lett.* **2022**, *7*, 1246–1254.

[118] Z. C. Yang, W. J. Zhang, S. H. Wu, H. M. Zhu, Z. H. Liu, Z. Y. Liu, Z. Y. Jiang, R. Chen, J. Zhou, Q. Lu, Z. W. Xiao, L. Shi, H. Chen, L. Ono, S. S. Zhang, Y. Q. Zhang, Y. B. Qi, L. Y. Han, W. Chen, *Sci. Adv.* **2021**, *7*, eabg3749.

[119] W. Zuo, M. M. Byranvand, T. Kodalle, M. Zohdi, J. Lim, B. Carlsen, T. Magorian Friedlmeier, M. Kot, C. Das, J. I. Flege, W. Zong, A. Abate, C. M. Sutter-Fella, M. Li, M. Saliba, *Adv. Mater.* **2023**, *35*, 2302889.

[120] Y. Du, Q. Tian, S. Wang, L. Yin, C. Ma, Z. Wang, L. Lang, Y. Yang, K. Zhao, S. Liu, *Adv. Mater.* **2024**, *36*, 2307583.

[121] T. Bu, J. Li, H. Li, C. Tian, J. Su, G. Tong, L. K. Ono, C. Wang, Z. Lin, N. Chai, X.-L. Zhang, J. Chang, J. Lu, J. Zhong, W. Huang, Y. Qi, Y.-B. Cheng, F. Huang, *Science* **2021**, *372*, 1327–1332.

[122] X. Huang, F. Cao, S. Zhan, Q. Feng, M. Zhu, Z. Su, X. Gao, J. Yin, J. Li, N. Zheng, B. Wu, *Joule* **2023**, *7*, 1556–1573.

[123] Y. Yang, Y. Wang, Z. Qu, K. Zhang, T. Liang, S. Chen, W. Lv, F. Min, Y. Chen, Y. Qiao, Y. Song, *Angew. Chem. Int. Ed.* **2023**, *62*, e202300971.

[124] H. Peng, D. Li, Z. Li, Z. Xing, X. Hu, T. Hu, Y. Chen, *Nano-Micro Lett.* **2023**, *15*, 91.

[125] J.-W. Lee, S. Tan, S. I. Seok, Y. Yang, N.-G. Park, *Science* **2022**, *375*, eabj1186.

[126] D. Y. Han, J. Wang, L. Agosta, Z. Zang, B. Zhao, L. M. Kong, H. Z. Lu, I. Mosquera-Lois, V. Carnevali, J. C. Dong, J. H. Zhou, H. Y. Ji, L. Pfeifer, S. M. Zakeeruddin, Y. G. Yang, B. Wu, U. Rothlisberger, X. Y. Yang, M. Grätzel, N. Wang, *Nature* **2023**, *622*, 493–498.

[127] M. Liu, T. Pauporté, *Nano-Micro Lett.* **2023**, *15*, 1–34.

[128] R. He, W. Wang, Z. Yi, F. Lang, C. Chen, J. Luo, J. Zhu, J. Thiesbrummel, S. Shah, K. Wei, Y. Luo, C. Wang, H. Lai, H. Huang, J. Zhou, B. Zou, X. Yin, S. Ren, X. Hao, L. Wu, J. Zhang, J. Zhang, M. Stolterfoht, F. Fu, W. Tang, D. Zhao, *Nature* **2023**, *618*, 80–86.

[129] C. Liang, H. Gu, Y. Xia, Z. Wang, X. Liu, J. Xia, S. Zuo, Y. Hu, X. Gao, W. Hui, L. Chao, T. Niu, M. Fang, H. Lu, H. Dong, H. Yu, S. Chen, X. Ran, L. Song, B. Li, J. Zhang, Y. Peng, G.

Shao, J. Wang, Y. Chen, G. Xing, W. Huang, *Nat. Energy* **2021**, *6*, 38–45.
[130] W. Hui, L. Chao, H. Lu, F. Xia, Q. Wei, Z. Su, T. Niu, L. Tao, B. Du, D. Li, Y. Wang, H. Dong, S. Zuo, B. Li, W. Shi, X. Ran, P. Li, H. Zhang, Z. Wu, C. Ran, L. Song, G. Xing, X. Gao, J. Zhang, Y. Xia, Y. Chen, W. Huang, *Science* **2021**, *371*, 1359–1364.
[131] Y. Shen, G. Xu, J. Li, X. Lin, F. Yang, H. Yang, W. Chen, Y. Wu, X. Wu, Q. Cheng, J. Zhu, Y. Li, Y. Li, *Angew. Chem. Int. Ed.* **2023**, *62*, e202300690.
[132] S. Bai, P. Da, C. Li, Z. Wang, Z. Yuan, F. Fu, M. Kawecki, X. Liu, N. Sakai, J. T.-W. Wang, S. Huettner, S. Buecheler, M. Fahlman, F. Gao, H. J. Snaith, *Nature* **2019**, *571*, 245–250.
[133] Y.-H. Lin, N. Sakai, P. Da, J. Wu, H. C. Sansom, A. J. Ramadan, S. Mahesh, J. Liu, R. D. J. Oliver, J. Lim, L. Aspitarte, K. Sharma, P. K. Madhu, A. B. Morales-Vilches, P. K. Nayak, S. Bai, F. Gao, C. R. M. Grovenor, M. B. Johnston, J. G. Labram, J. R. Durrant, J. M. Ball, B. Wenger, B. Stannowski, H. J. Snaith, *Science* **2020**, *369*, 96–102.
[134] Y. Liu, C. Tang, A. Sun, R. Zhuang, Y. Zheng, C. Tian, X. Wu, Z. Li, B. Ouyang, J. Du, Z. Li, Y. Hua, C.-C. Chen, *Mater. Horiz.* **2023**, *10*, 5763–5774.
[135] B. Ding, Y. Ding, J. Peng, J. Romano-deGea, L. E. K. Frederiksen, H. Kanda, O. A. Syzgantseva, M. A. Syzgantseva, J.-N. Audinot, J. Bour, S. Zhang, T. Wirtz, Z. Fei, P. Dörflinger, N. Shibayama, Y. Niu, S. Hu, S. Zhang, F. F. Tirani, Y. Liu, G.-J. Yang, K. Brooks, L. Hu, S. Kinge, V. Dyakonov, X. Zhang, S. Dai, P. J. Dyson, M. K. Nazeeruddin, *Nature* **2024**, *628*, 299–305.
[136] Y. Ding, B. Ding, P. Shi, J. Romano-deGea, Y. Li, R. C. Turnell-Ritson, O. A. Syzgantseva, I. Yavuz, M. Xia, R. Yu, M. A. Syzgantseva, J.-N. Audinot, X. Miao, X. Liao, J. Li, P. Dörflinger, V. Dyakonov, C. Liu, Y. Yang, L. Tao, K. G. Brooks, A. Slonopas, J. Pan, L. Zhang, Q. An, Y. Rong, J. Peng, L. Ding, E. Shi, L. Mai, S. Dai, K. Zhao, J. Sheng, R. Wang, P. J. Dyson, M. K. Nazeeruddin, *Science* **2024**, *386*, 531–538.
[137] X. Li, D. Q. Bi, C. Y. Yi, J. D. Decoppet, J. S. Luo, S. M. Zakeeruddin, A. Hagfeldt, M. Grätzel, *Science* **2016**, *353*, 58–62.
[138] G. Yu, K.-J. Jiang, W.-M. Gu, Y. Li, Y. Lin, Y. Xu, X. Jiao, T. Xue, Y. Zhang, Y. Song, *Angew. Chem. Int. Ed.* **2022**, *61*, e202203778.
[139] S. S. Mali, J. V. Patil, P. S. Shinde, G. de Miguel, C. K. Hong, *Matter* **2021**, *4*, 635–653.
[140] X. Dai, S. Chen, H. Jiao, L. Zhao, K. Wang, Z. Ni, Z. Yu, B. Chen, Y. Gao, J. Huang, *Nat. Energy* **2022**, *7*, 923–931.
[141] M. Du, X. Zhu, L. Wang, H. Wang, J. Feng, X. Jiang, Y. Cao, Y. Sun, L. Duan, Y. Jiao, K. Wang, X. Ren, Z. Yan, S. Pang, S. Liu, *Adv. Mater.* **2020**, *32*, 2004979.
[142] Q. Jiang, J. H. Tong, R. A. Scheidt, X. M. Wang, A. E. Louks, Y. M. Xian, R. Tirawat, A. F. Palmstrom, M. P. Hautzinger, S. P. Harvey, S. Johnston, L. T. Schelhas, B. W. Larson, E. L. Warren, M. C. Beard, J. J. Berry, Y. F. Yan, K. Zhu, *Science* **2022**, *378*, 1295–1300.
[143] Z. Li, X. Wang, Z. Wang, Z. Shao, L. Hao, Y. Rao, C. Chen, D. Liu, Q. Zhao, X. Sun, C. Gao, B. Zhang, X. Wang, L. Wang, G. Cui, S. Pang, *Nat. Commun.* **2022**, *13*, 4417.
[144] F. Li, C. Zhang, J.-H. Huang, H. Fan, H. Wang, P. Wang, C. Zhan, C.-M. Liu, X. Li, L.-M. Yang, Y. Song, K.-J. Jiang, *Angew. Chem. Int. Ed.* **2019**, *58*, 6688–6692.
[145] H. Fan, F. Li, P. Wang, Z. Gu, J.-H. Huang, K.-J. Jiang, B. Guan, L.-M. Yang, X. Zhou, Y. Song, *Nat. Commun.* **2020**, *11*, 5402.
[146] D.-N. Jeong, D.-K. Lee, S. Seo, S. Y. Lim, Y. Zhang, H. Shin, H. Cheong, N.-G. Park, *ACS Energy Lett.* **2019**, *4*, 1189–1195.
[147] J. Wang, S. Luo, X. Tang, S. Xiao, Z. Chen, S. Pang, L. Zhang, Y. Lin, J. He, Y. Yuan, *ACS Energy Lett.* **2021**, *6*, 3634–3642.
[148] Y. Luo, K. Liu, L. Yang, W. Feng, L. Zheng, L. Shen, Y. Jin, Z. Fang, P. Song, W. Tian, P. Xu, Y. Li, C. Tian, L. Xie, Z. Wei, *Nat. Commun.* **2023**, *14*, 3738.
[149] X. Zhao, P. Zhang, T. Liu, B. Tian, Y. Jiang, J. Zhang, Y. Tang, B. Li, M. Xue, W. Zhang, Z. Zhang, W. Guo, *Science* **2024**, *385*, 433–438.
[150] K. Liu, Y. Luo, Y. Jin, T. Liu, Y. Liang, L. Yang, P. Song, Z. Liu, C. Tian, L. Xie, Z. Wei, *Nat. Commun.* **2022**, *13*, 4891.
[151] J. Cao, X. Zhang, Y. Miao, W. Li, X. Zeng, S. Yang, C. Yan, J. Lu, W. Yang, *Matter* **2024**, *7*, 3728–3755.
[152] L. Li, H. Rao, Z. Wu, J. Hong, J. Zhang, Z. Pan, X. Zhong, *Adv. Funct. Mater.* **2024**, *34*, 2308428.
[153] S.-C. Feng, Y. Shen, X.-M. Hu, Z.-H. Su, K. Zhang, B.-F. Wang, L.-X. Cao, F.-M. Xie, H.-Z. Li, X. Gao, J.-X. Tang, Y.-Q. Li, *Adv. Mater.* **2024**, *36*, 2410255.
[154] J. Kong, Y. Shin, J. A. Röhr, H. Wang, J. Meng, Y. Wu, A. Katzenberg, G. Kim, D. Y. Kim, T.-D. Li, E. Chau, F. Antonio, T. Siboonruang, S. Kwon, K. Lee, J. R. Kim, M. A. Modestino, H. Wang, A. D. Taylor, *Nature* **2021**, *594*, 51–56.
[155] S. A. Johnson, K. P. White, J. Tong, S. You, A. Magomedov, B. W. Larson, D. Morales, R. Bramante, E. Dunphy, R. Tirawat, C. L. Perkins, J. Werner, G. Lahti, C. Velez, M. F. Toney, K. Zhu, M. D. McGehee, J. J. Berry, A. F. Palmstrom, *Joule* **2023**, *7*, 2873–2893.
[156] R. Azmi, D. S. Utomo, B. Vishal, S. Zhumagali, P. Dally, A. M. Risqi, A. Prasetio, E. Ugur, F. Cao, I. F. Imran, A. A. Said, A. R. Pininti, A. S. Subbiah, E. Aydin, C. Xiao, S. Il Seok, S. De Wolf, *Nature* **2024**, *628*, 93–98.
[157] R. Lin, Y. Wang, Q. Lu, B. Tang, J. Li, H. Gao, Y. Gao, H. Li, C. Ding, J. Wen, P. Wu, C. Liu, S. Zhao, K. Xiao, Z. Liu, C. Ma, Y. Deng, L. Li, F. Fan, H. Tan, *Nature* **2023**, *620*, 994–1000.
[158] S. Wang, Y. Jiang, E. J. Juarez-Perez, L. K. Ono, Y. Qi, *Nat. Energy* **2016**, *2*, 16195.
[159] J. Nespoli, M. Mugge, L. M. van der Poll, S. Lal, B. Ibrahim, B. Boshuizen, V. M. Caselli, A. J. Houtepen, L. J. Bannenberg, T. J. Savenije, *J. Am. Chem. Soc.* **2024**, *146*, 30860–30870.
[160] Z. Zhou, Z. Wang, Y. Zhou, S. Pang, D. Wang, H. Xu, Z. Liu, N. P. Padture, G. Cui, *Angew. Chem. Int. Ed.* **2015**, *127*, 9841–9845.
[161] J. Wen, Y. Zhao, Z. Liu, H. Gao, R. Lin, S. Wan, C. Ji, K. Xiao, Y. Gao, Y. Tian, J. Xie, C. J. Brabec, H. Tan, *Adv. Mater.* **2022**, *34*, 2110356.
[162] Y. Sun, Q. Yao, W. Xing, H. Jiang, Y. Li, W. Xiong, W. Zhu, Y. Zheng, *Adv. Sci.* **2023**, *10*, 2205986.
[163] J. Yuan, X. Zhang, D. Zhou, F. Ge, J. Zhong, S. Zhao, Z. Ou, G. Zhan, X. Zhang, C. Li, J. Tang, Q. Bai, J. Zhang, C. Zhu, T. Wang, L. Ruan, C. Zhu, X. Song, W. Huang, L. Wang, *Angew. Chem. Int. Ed.* **2023**, *62*, e202218546.
[164] K. Liu, H. Qi, R. Dong, R. Shivhare, M. Addicoat, T. Zhang, H. Sahabudeen, T. Heine, S. Mannsfeld, U. Kaiser, Z. Zheng, X. Feng, *Nat. Chem.* **2019**, *11*, 994–1000.
[165] F. Wang, J.-H. Seo, G. Luo, M. B. Starr, Z. Li, D. Geng, X. Yin, S. Wang, D. G. Fraser, D. Morgan, Z. Ma, X. Wang, *Nat. Commun.* **2016**, *7*, 10444.
[166] B. Chen, K. Meng, Z. Qiao, Y. Zhai, R. Yu, Z. Fang, P. Yan, M. Xiao, L. Pan, L. Zheng, K. Cao, G. Chen, *Adv. Mater.* **2024**, *36*, 2312054.
[167] M. Li, M. Liu, F. Qi, F. R. Lin, A. K. Y. Jen, *Chem. Rev.* **2024**, *124*, 2138–2204.
[168] L. Li, Y. Wang, X. Wang, R. Lin, X. Luo, Z. Liu, K. Zhou, S. Xiong, Q. Bao, G. Chen, Y. Tian, Y. Deng, K. Xiao, J. Wu, M. I. Saidaminov, H. Lin, C.-Q. Ma, Z. Zhao, Y. Wu, L. Zhang, H. Tan, *Nat. Energy* **2022**, *7*, 708–717.
[169] S. Liu, J. Li, W. Xiao, R. Chen, Z. Sun, Y. Zhang, X. Lei, S. Hu, M. Kober-Czerny, J. Wang, F. Ren, Q. Zhou, H. Raza, Y. Gao, Y. Ji, S. Li, H. Li, L. Qiu, W. Huang, Y. Zhao, B. Xu, Z. Liu, H. J. Snaith, N.-G. Park, W. Chen, *Nature* **2024**, *632*, 536–542.
[170] R. He, W. H. Wang, Z. J. Yi, F. Lang, C. Chen, J. C. Luo, J. W. Zhu, J. Thiesbrummel, S. Shah, K. Wei, Y. Luo, C. L. Wang, H. G. Lai, H. Huang, J. Zhou, B. S. Zou, X. X. Yin, S. Q. Ren, X.

Hao, L. L. Wu, J. Q. Zhang, J. B. Zhang, M. Stolterfoht, F. Fu, W. H. Tang, D. W. Zhao, *Nature* **2023**, *618*, 80–86.
[171] Z. H. Dai, S. K. Yadavalli, M. Chen, A. Abbaspourtamijani, Y. Qi, N. P. Padture, *Science* **2021**, *372*, 618–622.
[172] S. Q. Yu, Z. Xiong, H. T. Zhou, Q. Zhang, Z. H. Wang, F. Ma, Z. H. Qu, Y. Zhao, X. B. Chu, X. W. Zhang, J. B. You, *Science* **2023**, *382*, 1399–1404.
[173] J. Li, M. Chen, C. Zhang, H. Dong, W. Lin, P. Zhuang, Y. Wen, B. Tian, W. Cai, X. Zhang, *Adv. Mater.* **2019**, *31*, 1902431.
[174] R. Azmi, D. S. Utomo, B. Vishal, S. Zhumagali, P. Dally, A. M. Risqi, A. Prasetio, E. Ugur, F. Cao, I. F. Imran, A. A. Said, A. R. Pininti, A. S. Subbiah, E. Aydin, C. Xiao, S. I. Seok, S. De Wolf, *Nature* **2024**, *628*, 93–98.
[175] S. Chen, X. Xiao, B. Chen, L. L. Kelly, J. Zhao, Y. Lin, M. F. Toney, J. Huang, *Sci. Adv.* **2021**, *7*, eabb2412.
[176] H. Hu, M. Singh, X. Wan, J. Tang, C.-W. Chu, G. Li, *J. Mater. Chem. A* **2020**, *8*, 1578–1603.
[177] J. Shi, W. Ge, Y. Tian, M. Xu, W. Gao, Y. Wu, *Small* **2021**, *17*, 2006568.
[178] N. Li, X. Niu, L. Li, H. Wang, Z. Huang, Y. Zhang, Y. Chen, X. Zhang, C. Zhu, H. Zai, Y. Bai, S. Ma, H. Liu, X. Liu, Z. Guo, G. Liu, R. Fan, H. Chen, J. Wang, Y. Lun, X. Wang, J. Hong, H. Xie, D. S. Jakob, X. G. Xu, Q. Chen, H. Zhou, *Science* **2021**, *373*, 561–567.
[179] H. Hu, D. B. Ritzer, A. Diercks, Y. Li, R. Singh, P. Fassl, Q. Jin, F. Schackmar, U. W. Paetzold, B. A. Nejand, *Joule* **2023**, *7*, 1574–1592.
[180] Y. Yang, H. Chen, C. Liu, J. Xu, C. Huang, C. D. Malliakas, H. Wan, A. S. R. Bati, Z. Wang, R. P. Reynolds, I. W. Gilley, S. Kitade, T. E. Wiggins, S. Zeiske, S. Suragtkhuu, M. Batmunkh, L. X. Chen, B. Chen, M. G. Kanatzidis, E. H. Sargent, *Science* **2024**, *386*, 898–902.
[181] S. Yu, Z. Xiong, H. Zhou, Q. Zhang, Z. Wang, F. Ma, Z. Qu, Y. Zhao, X. Chu, X. Zhang, J. You, *Science* **2023**, *382*, 1399–1404.
[182] H. Li, L. Tan, C. Jiang, M. Li, J. Zhou, Y. Ye, Y. Liu, C. Yi, *Adv. Funct. Mater.* **2023**, *33*, 2211232.
[183] F. U. Kosasih, E. Erdenebileg, N. Mathews, S. G. Mhaisalkar, A. Bruno, *Joule* **2022**, *6*, 2692–2734.
[184] L. Tan, J. Zhou, X. Zhao, S. Wang, M. Li, C. Jiang, H. Li, Y. Zhang, Y. Ye, W. Tress, L. Ding, M. Grätzel, C. Yi, *Adv. Mater.* **2023**, *35*, 2205027.
[185] L.-H. Chou, J. M. W. Chan, C.-L. Liu, *Sol. RRL* **2022**, *6*, 2101035.
[186] C. Wu, K. Wang, Y. Jiang, D. Yang, Y. Hou, T. Ye, C. S. Han, B. Chi, L. Zhao, S. Wang, W. Deng, S. Priya, *Adv. Funct. Mater.* **2021**, *31*, 2006803.
[187] J. E. Bishop, C. D. Read, J. A. Smith, T. J. Routledge, D. G. Lidzey, *Sci. Rep.* **2020**, *10*, 6610.
[188] N. Rolston, W. J. Scheideler, A. C. Flick, J. P. Chen, H. Elmaraghi, A. Sleugh, O. Zhao, M. Woodhouse, R. H. Dauskardt, *Joule* **2020**, *4*, 2675–2692.
[189] J. H. Heo, F. Zhang, C. Xiao, S. J. Heo, J. K. Park, J. J. Berry, K. Zhu, S. H. Im, *Joule* **2021**, *5*, 481–494.
[190] J. Li, J. Dagar, O. Shargaieva, O. Maus, M. Remec, Q. Emery, M. Khenkin, C. Ulbrich, F. Akhundova, J. A. Márquez, T. Unold, M. Fenske, C. Schultz, B. Stegemann, A. Al-Ashouri, S. Albrecht, A. T. Esteves, L. Korte, H. Köbler, A. Abate, D. M. Többens, I. Zizak, E. J. W. List-Kratochvil, R. Schlatmann, E. Unger, *Adv. Energy Mater.* **2023**, *13*, 2203898.
[191] P. J. S. Rana, B. Febriansyah, T. M. Koh, B. T. Muhammad, T. Salim, T. J. N. Hooper, A. Kanwat, B. Ghosh, P. Kajal, J. H. Lew, Y. C. Aw, N. Yantara, A. Bruno, S. A. Pullarkat, J. W. Ager, W. L. Leong, S. G. Mhaisalkar, N. Mathews, *Adv. Funct. Mater.* **2022**, *32*, 2113026.
[192] T. R. Rana, M. Abbas, E. Schwartz, F. Jiang, M. Y. Yaman, Z. Xu, D. S. Ginger, D. MacKenzie, *ACS Energy Lett.* **2024**, *9*, 1888–1894.
[193] L. Wang, D. Zheng, Z. Li, B. Farhadi, L. Peng, S. Zhao, Z. Chang, L. Duan, Y. Cao, H. Wang, Y. Tong, M. Du, K. Wang, S. Liu, *Matter* **2023**, *6*, 2987–3005.
[194] J. W. Yoo, E. Noh, J. Jang, K. S. Lee, J. Byeon, M. Choi, J. Im, S. I. Seok, *Joule* **2023**, *7*, 797–809.
[195] Z. Yang, W. Zhang, S. Wu, H. Zhu, Z. Liu, Z. Liu, Z. Jiang, R. Chen, J. Zhou, Q. Lu, Z. Xiao, L. Shi, H. Chen, L. K. Ono, S. Zhang, Y. Zhang, Y. Qi, L. Han, W. Chen, *Sci. Adv.* **2021**, *7*, eabg3749.
[196] W. Feng, J. Tao, G. Liu, G. Yang, J.-X. Zhong, Y. Fang, L. Gong, S. Yang, W.-Q. Wu, *Angew. Chem. Int. Ed.* **2023**, *62*, e202300265.
[197] Q. Liang, K. Liu, M. Sun, Z. Ren, P. W. K. Fong, J. Huang, M. Qin, Z. Wu, D. Shen, C.-S. Lee, J. Hao, X. Lu, B. Huang, G. Li, *Adv. Mater.* **2022**, *34*, 2200276.
[198] H. Gao, K. Xiao, R. Lin, S. Zhao, W. Wang, S. Dayneko, C. Duan, C. Ji, H. Sun, A. D. Bui, C. Liu, J. Wen, W. Kong, H. Luo, X. Zheng, Z. Liu, H. Nguyen, J. Xie, L. Li, M. I. Saidaminov, H. Tan, *Science* **2024**, *383*, 855–859.
[199] K. Xiao, Y.-H. Lin, M. Zhang, R. D. J. Oliver, X. Wang, Z. Liu, X. Luo, J. Li, D. Lai, H. Luo, R. Lin, J. Xu, Y. Hou, H. J. Snaith, H. Tan, *Science* **2022**, *376*, 762–767.
[200] H. Wang, S. Su, Y. Chen, M. Ren, S. Wang, Y. Wang, C. Zhu, Y. Miao, C. Ouyang, Y. Zhao, *Nature* **2024**, *634*, 1091–1095.
[201] C. Chen, C. Ran, C. Guo, Q. Yao, J. Wang, T. Niu, D. Li, L. Chao, Y. Xia, Y. Chen, *Adv. Energy Mater.* **2023**, *13*, 2302654.
[202] C. Chen, C. Ran, Q. Yao, J. Wang, C. Guo, L. Gu, H. Han, X. Wang, L. Chao, Y. Xia, Y. Chen, *Adv. Sci.* **2023**, *10*, 2303992.
[203] M. A. Uddin, P. J. S. Rana, Z. Ni, X. Dai, Z. Yu, Z. Shi, H. Jiao, J. Huang, *Adv. Mater.* **2022**, *34*, 2202954.
[204] J. Liu, X. Chen, K. Chen, W. Tian, Y. Sheng, B. She, Y. Jiang, D. Zhang, Y. Liu, J. Qi, K. Chen, Y. Ma, Z. Qiu, C. Wang, Y. Yin, S. Zhao, J. Leng, S. Jin, W. Zhao, Y. Qin, Y. Su, X. Li, X. Li, Y. Zhou, Y. Zhou, F. Ling, A. Mei, H. Han, *Science* **2024**, *383*, 1198–1204.

Manuscript received: February 12, 2025
Revised manuscript received: March 20, 2025
Accepted manuscript online: March 20, 2025
Version of record online: March 27, 2025